공학박사 학위논문

Frequency Tracking Methods for GPS Chirp-Type Interference Detection and Mitigation

위성항법시스템 전파간섭 검출 및 완화를 위한

전파간섭 신호 주파수 추적 기법

2016 년 8 월

서울대학교 대학원

기계항공공학부

강 창 호

Abstract

Frequency Tracking Methods for GPS Chirp-Type Interference Detection and Mitigation

Chang Ho Kang
Department of Mechanical & Aerospace Engineering
The Graduate School
Seoul National University

The potential threat of GPS interference has arisen with the increased reliability on GPS and the open availability of portable jammers online at present. In order to deal with this threat, detecting and tracking interference are important for safe GPS operations in all countries. Previous works have focused on detecting the existence of interference using an adaptive notch filter. These approaches are limited when used to detect and track chirp-type interference because the fast sweep rate of this type of interference degrades the signal tracking performance of an adaptive notch filter. Nevertheless, when the adaptation parameters are properly selected, the adaptive notch filter can track and mitigate the jamming signals. This method also has limitations when the quality of the measurement suddenly deteriorates or the sweep rate changes. In this case, the tracking and mitigation performance of the adaptive

notch filter is degraded on account of the simple filter structure, which does not include a robust algorithm. Thus, it is necessary to use a model-based tracking algorithm for chirp-type interference when the measurement noise increases.

In this dissertation, two Kalman filtering based methods are proposed to design the model-based tracking algorithm for chirp-type interference as well as other continuous wave interference. By using the estimated frequency, mitigation algorithm is also proposed and is based on the second order digital notch filter.

The frequency of GPS interference can be obtained using the properties of the trigonometric functions of received signal samples, but these values contain numerous errors caused by measurement noise and frequency changes associated with the interference. In order to reduce these errors, an adaptive fading Kalman filter with a low-pass differentiator (LPD) and a pattern enhancement algorithm is used to estimate the sweep period of chirp-type interference, which is used to reset the filter parameter for estimating the frequency of the interference accurately. By estimating the sweep period, the interference identification logic is designed to select the proper system model of the Kalman filter.

However, due to the limited performance of LPD which is used to estimate the sweep period of the interference, the algorithm can only track linear chirp-type interference which has a dramatic change at the end of sweep period. In order to deal with the problem, the revised frequency tracking algorithm which does not depend on estimating the sweep period is needed to

track the various chirp-type interferences. Thus, the frequency of chirp-type interference is modeled by a Fourier series, which is always valid regardless of the sweep period and which can maintain tracking performance better than the previous methods when nonlinear chirp-type interference is received. In addition, an optimization technique based on Powell's method is applied to the main algorithm in order to select the optimal number of coefficients.

Finally, in order to mitigate the interference, the estimated frequency from the filter is used to design a notch filter which eliminates the interference in the received signal. The mitigation performance of the proposed algorithm is evaluated by means of Monte-Carlo simulations. The performance of the proposed algorithm is simulated for scenarios of GPS signals in the presence of various chirp-type interference and is analyzed by using software GPS and interference simulator data. Through theoretical analysis and by comparing simulation results with conventional algorithms, the feasibility and performance of the proposed methods are shown.

Keywords: GPS interference detection and mitigation, adaptive Kalman filter, adaptive notch filter, Fourier analysis, pattern enhancement

Student Number: 2009-23059

Contents

List of Tables

List of Figures

Chapter 1. Introduction

1.1 Motivation and Background

GNSS are space-based satellite navigation systems that provide autonomous geo-spatial positioning with global coverage. In order to send the information of satellites to GNSS receivers on the ground, the navigation system uses a radio frequency (RF) signal. However, its received signal power is relatively weak, because of the long distance between satellites and GNSS receivers. For this reason, it is easy for other RF signal sources to degrade the performance of GNSS receivers, by making acquisition and tracking of the satellite signals difficult or impossible. In particular, an intentional RF signal that degrades the navigation accuracy or causes a complete loss of receiver tracking is called a GNSS interference or jamming signal. Such interference is a major threat to civil aviation using GNSS [1].

In the past five years, South Korea has, on several occasions, experienced intentional GPS jamming. By investigation, it was found that the incident was due to intentional jamming by North Korea, and the types of jamming signals were single-tone continuous wave on L1, and swept continuous wave on L2 and L5 frequency bands [2, 3]. Seoul/Incheon International Airport, the largest airport in South Korea, is only about 50 km away from the Demilitarized Zone (DMZ), so GPS jammers in place near the DMZ can easily disrupt GPS signals in Incheon International Airport.

Therefore, detecting and characterizing interference, and giving timely alert are important for GNSS operation in South Korea, as it is in all countries [4].

The performance of a GNSS receiver will be severely degraded as the interference signal's power level becomes stronger than the system's anti-jamming ability can endure [5]. Previous works presented that for a given power, one of the most effective interference sources is continuous wave interference [6]. Continuous wave interference (CWI) can easily overwhelm a GNSS receiver's analog-to-digital converter at the analog front-end part, and paralyze the GNSS receiver. In addition, even weak CWI slightly above the specified RFI mask can degrade the signal quality and positional accuracy of the receiver. Therefore, CWI detection and mitigation methods by adaptive filtering techniques have attracted considerable attention. Detection and mitigation methods of CWI by using an adaptive filter have been studied constantly and can be classified into two approaches: time-domain and frequency-domain approaches. In the time-domain approach, Cho and Lee [7] and Choi and Cho [8] presented simple methods for retrieving a single-tone CWI, by using an adaptive IIR notch filter based on the lattice form. An enhanced nonlinear prediction technique is proposed to suppress interferences [9]. Borio [10] designed a method to estimate the existence of CWI using the property that zeros of the adaptive notch filter are placed close to the unit circle when the interference is received. In a similar manner, Chien [11] proposed a detection method of GNSS CWI using the variance of estimated frequency. In the frequency domain, Capozza [12] proposed an N-sigma excision method to reject CWI. Balaei and Dempster [13] devised a statistical

hypothesis testing method to detect GPS CWI in the frequency domain. Previous works have focused on detecting the existence of CWI using an adaptive notch filter.

These approaches are limited when used to detect and track chirp-type interference because the fast sweep rate of this type of interference degrades the signal tracking performance of an adaptive notch filter. However, when the adaptation parameters are properly selected, the adaptive notch filter can track the jamming signals and mitigate the signal. In one study [14], the authors proposed an IIR adaptive notch filter as a means to implement a tracking and mitigation technique for chirp signals. The capabilities of the notch filter were experimentally analyzed through a series of experiments, but this method also has limitations when the quality of the measurement suddenly deteriorates or the sweep rate changes. In these cases, the tracking and mitigation performance of the adaptive notch filter is degraded on account of the simple filter structure, which does not include a robust algorithm. Thus, it is necessary to use a model-based tracking algorithm for chirp-type interference when the measurement noise increases.

The adaptive fading Kalman filter is applied and a pattern recognition algorithm with a low pass differentiator (LPD) is used to estimate the sweep period of chirp-type GNSS interference to reset the filter parameter for improving the frequency tracking performance. The adaptive fading Kalman filter is one of adaptive filtering methods for reducing abnormal measurement error by adjusting Kalman gain. Thus, using the adaptive fading Kalman filter is expected to reduce the measurement error caused by the trigonometric

functions and measurement noise. Interference identification logic is also proposed to classify the type of interference using the pulsed signal generated by the pattern recognition algorithm and to select the proper filter model of the Kalman filter for frequency tracking. However, due to the limited performance of LPD which is used to estimate the sweep period of the interference, the algorithm can only track linear chirp-type interference which has a dramatic change at the end of sweep period. If another chirp-type which does not have the dramatic change at the end of sweep period is received, the LPD cannot recognize the sweep period of the different chirp-type interference. Furthermore, as a constant rate of frequency change model is used, a frequency tracking error may occur when the frequency change rate is not constant in the sweep period.

In order to deal with these problems, the revised frequency tracking algorithm which does not depend on estimating the sweep period is needed, to track the various chirp-type interferences. And a nonlinear frequency-tracking model is also needed to reduce the tracking error. Thus, the frequency of chirp-type interference is modeled by a Fourier series, which is always valid regardless of the sweep period and which can maintain tracking performance better than the previous method [15] when nonlinear chirp-type interference is received. The coefficients of the Fourier series are estimated by an adaptive fading Kalman filter, for applying to real-time systems and maintaining frequency tracking performance when measurement error occurs. In addition, an optimization technique based on Powell's method is applied to the main algorithm in order to select the optimal number of coefficients.

1.2 Objective and Contributions

The main goal of this dissertation is to improve the tracking performance of GNSS interference in order to mitigate its effect on GNSS signal quality. The objectives in this study are summarized as follows:

- Analysis on characteristics of recent GPS interference
- Improving a frequency tracking performance than conventional algorithms
- Developing an adaptive filtering method, in order to estimate the interference frequency accurately when measurement error occurs
- Developing a mitigation algorithm based on the notch filter for reducing the effect of the GPS interference

The proposed algorithms consider the above issues and original contributions of this study are as follows:

- In the case of linear chirp-type interference, an interference identification and tracking algorithm which uses an adaptive fading Kalman filter, a pattern recognition algorithm with LPD, and a pattern enhancement algorithm based on the AR model is proposed. The selection method of the filter model according to the type of interference and the reinitialization of the filter parameter are also proposed to improve the interference frequency tracking result. The

performance of the proposed algorithm is verified in terms of frequency tracking by comparing its results to those of conventional algorithms.

- In the case of various type interference, an interference tracking algorithm is proposed that utilizes an adaptive hybrid EKF that is based on the Fourier series and also an order-reduction algorithm based on Powell's method to estimate the frequency of various chirp-type interferences. The proposed adaptive logic always guarantees the nonnegative aspect of the fading factor and reduces the measurement error effectively. In addition, the optimal order of the Fourier series for the signal type is selected by the proposed order-reduction algorithm. Simulation results show that, compared to conventional methods, the proposed algorithm can more efficiently track various types of chirp interference.
- The requirement of the mitigation algorithm using the notch filter is determined through the Monte Carlo simulations and the adjustment parameter of notch depth is added to the general notch filter in order to reduce GPS data distortion while removing the interference effectively.

1.3 Organization

Chapter 1 is the introduction, which summarizes objective and contribution of this dissertation with motivation and background.

Chapter 2 reviews the signal model of GPS and GPS interference in intermediate frequency bandwidth. In addition, interference frequency model is also introduced.

Chapter 3 describes three algorithms of GPS interference frequency tracking. In the first, adaptive lattice IIR notch filter based algorithm is reviewed. In the second, a Kalman filter based method with periodic reinitialization of filter states is proposed. In order to reinitialize the filter states, a pattern recognition algorithm with LPD is used and its properties are analyzed in this section. In the last, an adaptive Kalman filter based method with the Fourier series is proposed. Order-reduction algorithm based on Powell's method for estimating the frequency of various chirp-type interferences efficiently is also explained.

Chapter 4 describes detection and mitigation algorithms of GPS interference. Characteristics of AGCgain and filter parameters which are used to detect GPS interference are analyzed. In addition a second-order digital notch filter which are used to mitigate GPS interference and adjustment of its notch depth are also explained. The mitigation performance of the proposed algorithm is evaluated by means of Monte-Carlo simulations

Finally, the conclusions are presented in Chapter 5

.

Chapter 2. Global Positioning System Interference

This chapter provides a brief introduction to types of GPS interference and the signal model of GPS with GPS interference in intermediate frequency bandwidth. In addition, representative interference frequency models such as single-tone and chirp-type are also explained.

2.1 Types of GPS Interference

In terms of signal specturm, GPS interference is normally categorized as either wideband or narrowband, depending on whether its bandwidth is wide or narrow relative to the bandwidth of the desired GNSS signal. In the case of the GPS L1 C/A signal, the bandwidth of the signal is 2.046 MHz. Thus, interference is classified as narrowband interference when its frequency bandwidth is less than 2.046 MHz. Otherwise, the interference is classified as wideband interference. In addition, types of interference are classified by its frequency and modulation characteristics. Table 2.1 shows types of radio frequency interference and potential sources [16]. Among those interference types, analysis of interference is focused on narrowband interference which is most frequently occurring interference type.

Another a means of classifying GPS interference is based on the intent of the GPS interference [17]. It is designed to better understand the many

possible sources of interference and their potential effects on GNSS. The categories are malicious interference, uninformed interference, and accidental interference. The first category, malicious interference refers to GPS interference that is intentionally transmitted to prevent the use of GNSS for as many users as possible. The second category is uninformed interference which results from the intentional transmission of signals at or near GNSS frequencies but without the desire to cause harm. The third category, accidental interference, results from unintentional transmissions at or near GNSS frequencies. This usually is due to malfunctions of equipment that is designed to transmit at other frequencies.

Now a days, personal privacy devices (PPDs) shown in figure 2.1 are the most prevalent sources of GPS interference in the U.S [18]. This name comes from the fact that the primary market for these devices consists of people who fear being tracked or monitored by GNSS in their vehicles while North Korea's intentional jammers are the main GPS interference threat to South Korea. However, PPDs and the intentional jammers have similar characteristics except for their transmitting powers.

Civilian GPS jammers can be found in a variety of form factors, but are on average approximately the size of a hand-held cell phone. Three different civilian GPS jammers are shown in figure 2.1[18]. The jammer on the far left in the picture is the lowest power jammer and is powered from an automobile accessory power outlet. The middle one is slightly more powerful, contains a battery, and can be carried around and activated at almost any location and time. The one on the farright is slightly less powerful than the middle one, but

it also contains a battery and is disguised to look like a cellular telephone.

Table 2.1 Types of GPS interference [16]

Class-Type	Potential Sources
Wideband-band-limited Gaussian	Intentional matched bandwidth noise jammers
Wideband-Phase/frequency modulation	Television transmitters' harmonics or near-band microwave link transmitters overcoming the front end filter of a GNSS receiver
Wideband-matched spectrum	Intentional matched-spectrum jammers, spoofers, or nearby pseudolites
Wideband-pulse	Any type of burst transmitters such as radar or ultrawideband(UWB)
Narrowband-phase/frequency modulation	Intentional chirp jammers or harmonics from an amplitude modulation(AM) radio station, citizens band(CB) radio, or amateur radio transmitter
Narrowband-swept continuous wave	Intentional swept CW jammers or frequency modulation (FM) stations transmitters' harmonics
Narrowband-continuous wave	Intentional CW jammers or near-band unmodulated transmitter's carriers

Figure 2.1 Personal privacy devices [18]

Processing of signals from GPS jammers can benefit from an understanding of the RF output of the jammers. A typical output of a civil GPS jammer is shown in figure 2.2 a). The horizontal axis is time and the top plot's vertical axis is frequency. Each vertical slice of the top plot in the figure is a Fast Fourier Transform (FFT) of the RF sampled signal, centered at the L1 frequency. The bottom plot's vertical axis is power. The figure shows a classic example of a chirp signal, or a tone whose frequency repeatedly ramps linearly upwards and then resets back to the starting frequency. In addition, characteristics of the chirp signal are also summarized in [18]. According to analysis in [18], the average sweep rate of the PPDs is near 1×10^{12} Hz/s which is calculated by sweep periods and sweep ranges of frequency written in [18]. The effect of the interference on GPS quality is already analyzed in [3]. The chirp-type interference has a severe effect on

the quality of GPS signal when jammer to signal ratio (J/S) is above 25 dB as shown in figure 2.2 b) [3].

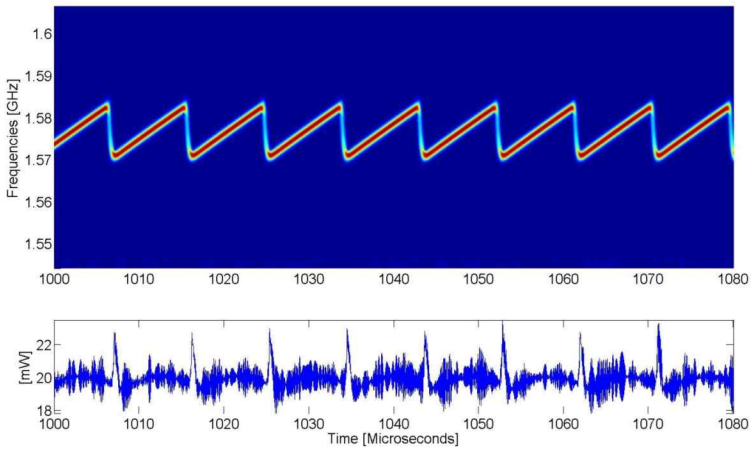

a) Frequency response of GPS jammer [18]

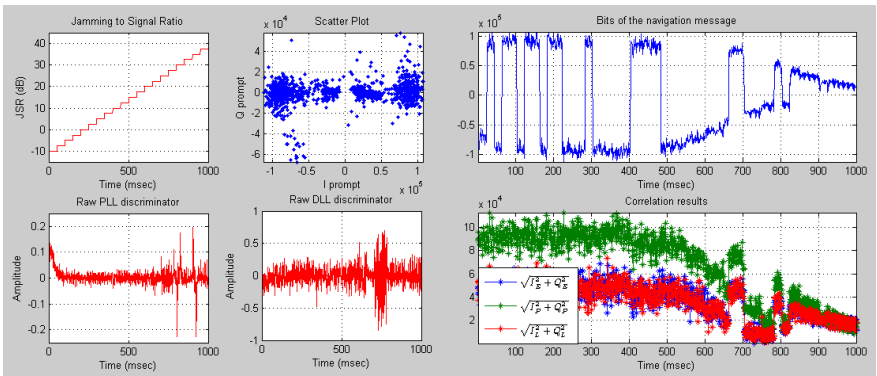

b) Effects of GPS chirp-type interference on GPS receiver [3]

Figure 2.2 Characteristics of GPS chirp-type interference

2.2 Overview of GPS Interference Mitigation Methods

Interference to civilian receivers is likely to increase in the future due to the rapid growth of telecommunications and other wireless data transmission systems. Although these systems may not transmit on the same frequency as GPS, intermodulation products and other out of band transmissions may lie in the GPS band [19]. Military users also need to consider intentional jamming. Due to the low powers required to jam GPS, jammers are cheap to build and a Russian jammer is currently being marketed [20].

Simple modifications to the A/D can improve the mitigation margins of the receiver against CW interferences. Post-correlation techniques involve modifications to the receiver tracking loops and can give limited additional protection against interferences. A major advantage of these schemes is that they are effective against all interference waveforms and require little, if any, modifications to the receiver hardware. Some can be implemented completely in software.

Pre-correlation techniques can be used to further improve the mitigation performance of the receiver. These techniques are applied prior to the tracking loops and can be packaged as an external system to existing GPS receivers. They usually require significant additional DSP processing power. Amplitude domain processing and temporal filtering techniques are the simplest to implement, as they only require a single antenna element. These techniques can be directly implemented to most current GPS receiver installations, but are only effective against narrow band interferences. Spatial filters are also effective against broadband interferences, but require an

antenna array. This significantly increases both the cost and size of the installation. Combined spatiotemporal filters achieve the best performance against both narrowband and broadband interferences but are also the most expensive to implement.

In this sections, some of representative mitigation algorithms are explained.

2.2.1 Post Correlation Techniques

Post correlation techniques are implemented within the GPS receiver tracking loops and improve the tracking thresholds. They can often be implemented through software changes, and do not significantly increase the power consumption of the GPS receiver.

Reducing the bandwidth of the carrier tracking loop increases its tracking threshold at a cost of degraded dynamic performance. By adaptively adjusting the tracking loop bandwidth, according to the interference power, higher mtigiation margins can be obtained under lower dynamics [16, 21, 22]. Simply switching to a much narrower tracking loop bandwidth when the receiver is stationary has also been tested and found to improve the carrier tracking threshold of the receiver by 10 dB [23].

In a standard GPS receiver, each tracking loop update occurs independently of the others. The outputs of the tracking loops are then combined in the navigation processor. Vector tracking loops integrate the tracking loops and navigation processor, such that each tracking loop update is also based on information from other tracking loops. The main advantage

of these techniques seems to be in situations where more than 4 satellites are visible. In this case common information from several satellites can be used to reinforce the signal strengths of the weaker ones [24]. Another approach is to use the common information from multiple GPS satellites to estimate the platform dynamics, which can then be used to aid the tracking loops, allowing them to operate at a reduced bandwidth, increasing their interference immunity [25].

In a tightly coupled GPS/INS system, the INS measurements can be used to aid the carrier tracking loops. This removes the dynamics from the loops and allows them to operate at a much narrower bandwidth. Typically, a factor of 10 reduction in bandwidth is achieved, resulting in an additional mitigation of 10 dB [16].

2.2.2 Pre Correlation Techniques

Precorrelation techniques can be used to achieve significant additional antijam margins. They are mainly implemented in digital signal processing (DSP) and can be applied either directly after the A/D converter.

Amplitude domain processing techniques modify the amplitude of each digital sample in such a way that nonGaussian interferences are suppressed, resulting in an overall improvement in SNR.

The adaptive algorithm, based on linear prediction, periodically captures a block of data from which the optimal FIR filter coefficients are calculated to notch out the interference. These coefficients are then downloaded to the FIR filter. The optimal filter will tend to maintain near

unity gain at all frequencies, apart from the interference frequency. As an example, consider the filter transfer function obtained from a multitoned interference. The adaptive algorithm was implemented on a DSP and took about 1 ms to complete 14 iterations.

The pre-correlation techniques are based on a single antenna element and could not reject broadband noise interferences. Spatial filters reject the interference in angle, rather than frequency, and can achieve large mitigation margins against most interference waveforms, including broadband noise. Spatial filters require multi element antenna arrays, which are significantly larger and heavier than single antenna elements. They can cancel up to N+1 interferences, where N is the number of antennas in the array.

In this dissertation, a pre-correlation method is selected to design the detection and mitigation method of GPS chirp-type interference because the pre-correlation method is more sensitive and effective to detect GPS chirp-type interference than post-correlation methods [3].

2.3 GPS and GPS interference model

A MATLAB SIMULINK-based GPS L1 signal and interference simulator is used to assess AGC gains and generate IF signal data in various interference scenarios [3]. The simulator generates a GPS L1 C/A signal, which is modeled as

$$r_n = \sqrt{2P} D_{n-\tau} c_{n-\tau} \cos\left(2\pi\left(f_{IF} + f_d\right)n + \theta\right) + v_n + i_n \tag{2.1}$$

where P is an intermediate frequency signal power, D_n is navigation data, c_n is a coarse acquisition code (C/A code) assigned to a GPS satellite, f_{IF} is an intermediate frequency of 9.548 MHz, f_d is the Doppler frequency shift, v_n is noise, i_n is interference, τ is the code phase of the received signal, and θ is the phase. $n = t / f_s$, where t is time and f_s is the sampling frequency of 38.192MHz.

Previous work [18] surveyed the signal properties of commercial GPS jammers based on experimental data. The tests of the jammers provided information on the characteristics of current civil GPS jammer signals. The majority of the jammers used chirp signals, all jammed L1 band, only six jammed the L2 band and none jammed the L5 band. The sweep rate of the jammers is on average about 1×10^{12} Hz/sec.

According to the results of the previous work, chirp-type GNSS interference is modeled as

$$i_{chirp\_n} = \sqrt{2P_i}\cos(2\pi n\left(S_{t\_n}\right) + \phi_i) \tag{2.2}$$

where P_i is the interference signal power, and ϕ_i is the initial phase. S_{t_n} can be expressed as follows:

$$S_{t\_n} = f_0 + \frac{a_i}{2f_s}n = f_0 + \frac{\Delta f}{2}n \tag{2.3}$$

where f_0 and α_i refer to the initial frequency and sweep rate of the interference, respectively. For simplicity, α_i / f_s is expressed by Δf which means the variation of digital frequency. n varies within the boundary T which is the sweep period of the chirp-type interference. The frequency of the linear chirp-type interference is modeled as

$$f_n = f_0 + \Delta f n \tag{2.4}$$

If n exceeds T, f_n changes from eq. 2.4 to

$$f_n = f_0 + \Delta f \times \left(n - T\right), \quad n \geq T \tag{2.5}$$

f_n is shown in figure 2.3. The sweep rate is set to 1×10^{12} Hz/sec and the initial digital frequency is 0.1832.

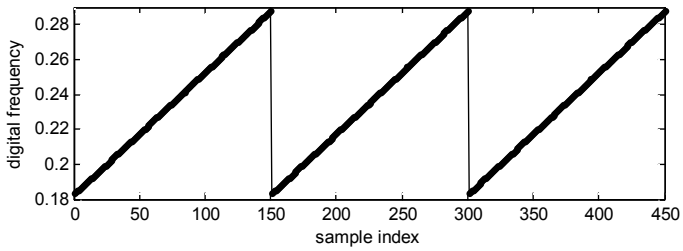

a) The chirp-type interference frequency

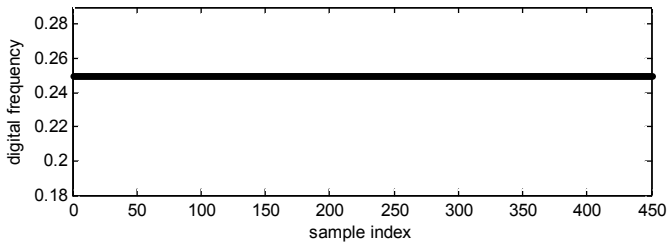

b) The single-tone CWI frequency

Figure 2.3 The frequency of the GNSS interference

Chapter 3. Interference Frequency Tracking

In this chapter, three algorithms of GPS interference frequency tracking. In the first, an adaptive lattice IIR notch filter based algorithm is reviewed. In the second, a Kalman filter based method with periodic reinitialization of filter states is proposed. In order to reinitialize the filter states, a pattern recognition algorithm with LPD is used and its properties are analyzed in this section. In the last, an adaptive Kalman filter based method with the Fourier series is proposed. Order-reduction algorithm based on Powell's method for estimating the frequency of various chirp-type interferences efficiently is also explained.

3.1 Adaptive Lattice IIR Notch Filter Based Method

In this section, the lattice IIR notch filter is briefly reviewed. The adaptive IIR notch filter has often been used to enhance sinusoids that have been corrupted by noise [7]. The IIR notch filter requires much less filter length than FIR filters, and it can remove the interference signal or narrow-band noise effectively [26]. In addition, it is shown that the lattice IIR notch filter provides better convergence properties, and more accurate frequency estimation compared to the direct form implementations [8].

An adaptive lattice IIR notch filter is used for the detection method, and the recursive least square (RLS) algorithm [7, 8] is used to estimate frequency. The transfer function of the notch filter can be represented as

$$H(z)=\frac{1-2\cos\omega_i z^{-1}+z^{-2}}{1-2(1+r)\cos\omega_i z^{-1}+rz^{-2}} \tag{3.1}$$

where, ω_i determines the notch frequency, and r is the distance between zero and pole.

The transfer function of the notch filter consists of two parts, as shown in figure 3.1, where $a=\cos(\omega_i)$. The first part is called the auto-regression (AR) block, whose role is to compensate for the effect of the moving average (MA) block [10] by raising the signal level near the interference frequency, so the filter can eliminate only the signal on the interference frequency. The second block refers to the MA block, which can remove not only the signal on the interference center frequency but also the signal located near the interference frequency where the transmitted data is located. Thus, as these two blocks are used simultaneously, the filter can eliminate only the signal on the interference frequency so that reduce the data loss. When the notch is placed at the frequency of the interference, the output power is minimized.

Therefore, the RLS algorithm uses the notch filter output power as a cost function,

$$J=E\left[y_n^2\right] \tag{3.2}$$

where, y_n is the output of the notch filter.

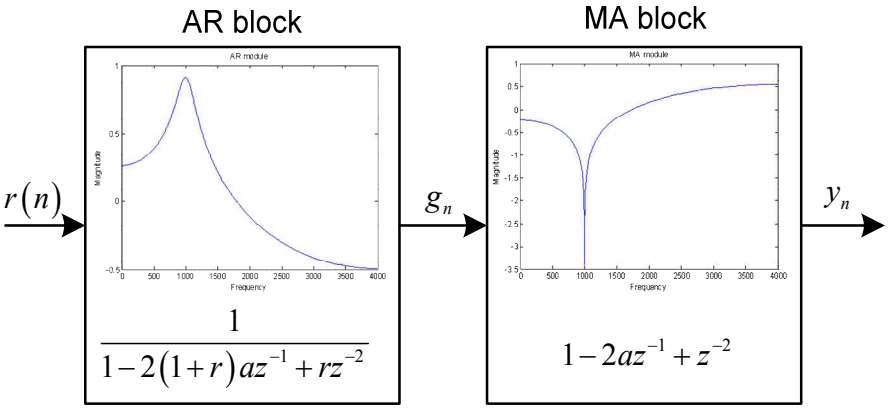

Figure 3.1 Adaptive IIR notch filter structure [26]

In order to find the parameter a that minimizes the cost function, the cost function is differentiated as

$$\begin{aligned}\frac{\partial J}{\partial a} &= E\left[2y_n\left(-2g_{n-1}\right)\right] \\ &= E\left[2\left(g_n - 2ag_{n-1} + g_{n-2}\right)\left(-2g_{n-1}\right)\right] = 0\end{aligned} \tag{3.3}$$

$$a(n) = \frac{E\left[g_{n-1}\left(g_n + g_{n-2}\right)\right]}{2E\left[g_{n-1}^2\right]} = \frac{r_1(n)}{r_0(n)} \tag{3.4}$$

$$r_1(n) = \lambda r_1(n-1) + (1-\lambda)\left(g_{n-1}\left(g_n + g_{n-2}\right)\right) \tag{3.5}$$

$$r_0(n) = \lambda r_0(n-1) + (1-\lambda)2g_{n-1}^2 \tag{3.6}$$

where, g_n is the output signal of the AR block, and λ is a forgetting factor for recursive calculation. For stability, a is clipped in the range of [-1,1], as shown in

$$a(n) = \begin{cases} a(n), & if\ -1 \le a(n) \le 1 \\ 1, & if\ \ a(n) > 1 \\ -1, & if\ \ a(n) < -1 \end{cases} \tag{3.7}$$

In addition, it is smoothed by

$$\hat{a}(n) = \gamma \hat{a}(n-1) + (\gamma - 1)a(n) \tag{3.8}$$

where, $\hat{a}(n)$ is the estimate of $a(n)$, and γ is the smoothing factor.

Since the normalized notch frequency f_n and a are related by $a = \cos(2\pi f_n)$, the frequency estimate at sample n is given by

$$\hat{f}_n(n) = \frac{1}{2\pi}\cos^{-1}\left(a(n)\right) \tag{3.9}$$

Adaptive notch filter based approaches have limitations in detecting and tracking chirp-type interference because the fast sweep rate of this interference degrades the signal tracking performance of an adaptive notch filter. However, if the adaptation parameters can be properly selected, the adaptive notch filter can track and mitigate the jamming signals. In [14], the authors proposed an IIR adaptive notch filter as a means to implement a tracking and mitigation technique for chirp signals. The capabilities of the notch filter were experimentally analyzed through a series of experiments, but this method also has limitations when the quality of the measurement suddenly deteriorates or the sweep rate changes. In these cases, the tracking and mitigation performance of the adaptive notch filter is degraded on account of the simple filter structure, which does not include a robust algorithm. Thus, it is necessary to use a model-based tracking algorithm for chirp-type interference when the measurement noise increases.

3.2 A Kalman Filter Based Method with Periodic Reinitialization of Filter States

The proposed frequency tracking algorithm uses the characteristics of the interference frequency according to the type of interference. In general, the single-tone CWI has a stationary frequency within narrow bandwidth, while the pertinent feature of chirp-type interference is that its frequency changes periodically. The chirp-type interference frequency increases linearly within one period and is reinitialized at the beginning of every period, as mentioned in the previous section. Thus, proper estimations of the initial frequency of interference, the sweep rate and the sweep period of the interference are very important to track the chirp-type interference. These values can also be used to identify the type of interference.

A Kalman filter is applied to the estimation frequency and sweep rate of the interference. A pattern recognition algorithm [18] with LPD [19] is also used to estimate the sweep period of the interference, and the pattern created by the pattern recognition algorithm is used to classify the interference into single-tone CWI or chirp-type interference. This type of identification improves the selection of a proper filter model for accurate frequency tracking.

Moreover, in order to improve the tracking performance of the filter, the state and the initial error covariance of the filter are reinitialized at the beginning of the estimated sweep period. The convergence speed of the filter is slower than the rate change of the chirp-type interference near the beginning of the sweep period. Thus, it is needed to reset the state and error covariance in order to track the chirp-type frequency. With the frequency

estimation results, it is possible to mitigate the effect of GNSS interference. A second-order digital IIR notch filter is applied to remove the GNSS interference; the center frequency of the notch is selected using the frequency tracking results.

The main structure of the proposed algorithm is shown in figure 3.2 [28]. It consists of four parts: the interference frequency calculation, interference identification, frequency tracking, and mitigation.

In the first step, the instantaneous frequency is calculated using the three samples of the received signal mentioned in the previous section.

In the second step, the LPD creates the peak pattern to estimate the sweep period of the chirp-type interference and to generate the pulsed signal used for the classification of the interference. The aforementioned pattern enhancement algorithm is also used to improve the peak detection performance, and the value of the enhanced peak pattern is utilized to generate the pulsed signal so that the type of interference can be labeled in the interference classification logic.

In the third step, the frequency tracking logic estimates the interference frequency using the interference identification result and the estimated time index of the sweep period from the previous step.

In the last step, the mitigation process is performed using the notch filter, whose notch center frequency is set with the frequency tracking results.

In this section, frequency tracking algorithm using the adaptive fading Kalman filter, the pattern recognition logic using the LPD, and the interference detection algorithm including the pattern enhancement algorithm

are explained. In addition, the mitigation algorithm based on the notch filter is also discussed.

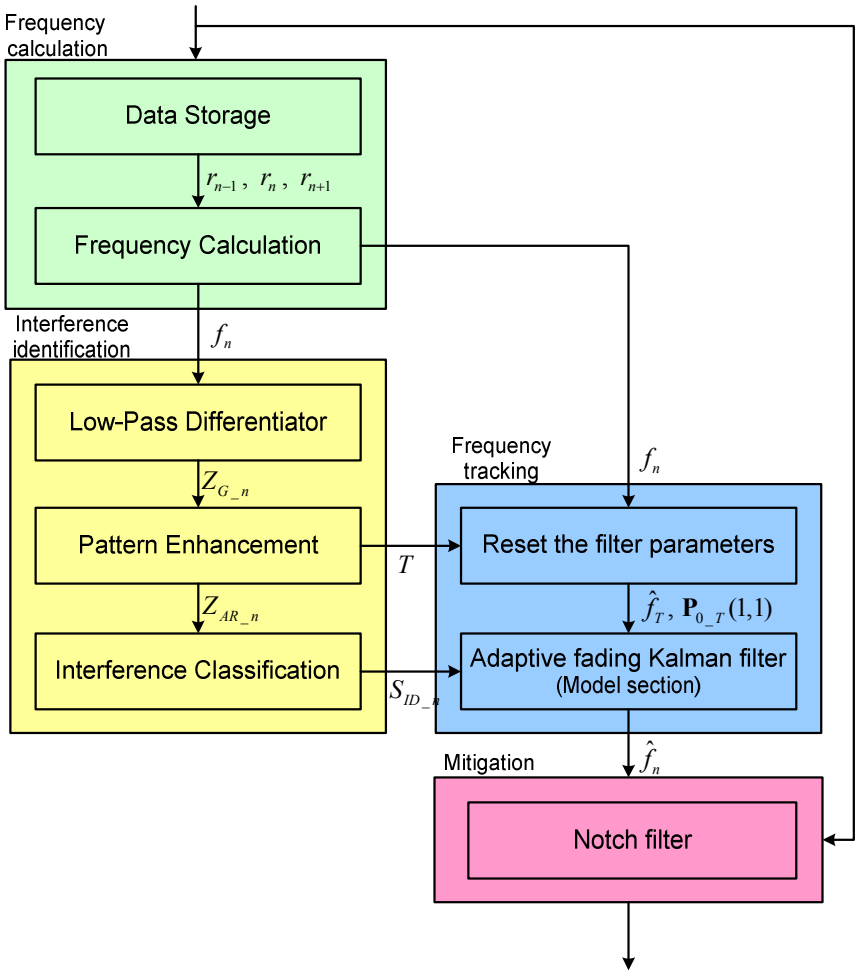

Figure 3.2 A flow chart of the proposed algorithm [28]

3.2.1 Instantaneous Frequency Calculation

The instantaneous frequency (IF) provides important information about changes in the frequency of non-stationary signals. The concept of IF is commonly used in various technical fields and applications, such as radar, sonar, and communications [29]. There are many means of estimating the IF estimation, including time-frequency representation approaches (linear, quadratic approaches) and IF estimation methods using analytic signals through the Hilbert transform. During the past five years, IF estimation methods based on these approaches have been modified and upgraded in an effort to improve the accuracy of these estimations. One of these methods, known as the S-transform, relies on a combination of short-time Fourier analysis and wavelet analysis. An S-transform-based IF estimator for signals with additive white Gaussian noise was proposed [30]. In this dissertation, the IF of chirp-type civilian GNSS interference is simply computed by summing received signal samples and by using the properties of trigonometric functions. Consequently this formula can generate IF estimation results rapidly and can be readily interpreted in a real-time system.

To estimate the frequency of the interference, three received samples (r_{n-1}, r_n, r_{n+1}) and a number of assumptions are needed. If the signal strength of i_n is greater than the GNSS signal and the measurement noise, the signal model of the received signal can be expressed as $r_n \approx i_n + v_n$. In general, GPS signal is very weak which is below the noise (-15~20dB) [31], while interference is stronger than noise and its jammer to noise ratio (J/S) is above 30dB in order to effect on GPS signal. In addition, if i_n is the chirp-type

interference and the measurement noise is ignored, the signal model of the three signal samples can be characterized as follows:

$$\begin{aligned} r_{n+1} &\approx \cos\left(2\pi\left(n+1\right)S_{t\_n+1}\right) \\ r_n &\approx \cos\left(2\pi n\left(S_{t\_n}\right)\right) \\ r_{n-1} &\approx \cos\left(2\pi\left(n-1\right)S_{t\_n-1}\right) \end{aligned} \tag{3.10}$$

Here, the interference signal power is assumed to be '1' and the initial phase is '0' for a convenient analysis. Assuming that $r_n \neq 0$ and $\Delta f = 0$, which refers to the single-tone CWI case [32], the frequency of the received signal can be calculated by the equation below.

$$\begin{aligned} \frac{r_{n+1}+r_{n-1}}{2r_n} &= \frac{\cos\left(2\pi\left(n+1\right)S_{t\_n+1}\right)+\cos\left(2\pi\left(n-1\right)S_{t\_n-1}\right)}{2\cos\left(2\pi n\left(S_{t\_n}\right)\right)} \\ &= \cos\left(2\pi\left(S_{t\_n}\right)\right) \end{aligned} \tag{3.11}$$

$$\therefore S_{t\_n} = f_n = \frac{1}{2\pi}\cos^{-1}\left(\frac{r_{n+1}+r_{n-1}}{2r_n}\right) \tag{3.12}$$

In this equation, $S_{t\_n} = f_n = f_0$, given that $\Delta f = 0$.

However, eq. 3.12 is not valid when $r_n = 0$, so that the measurement of the frequency cannot be obtained continuously. As r_n is the value of the periodic function, this problem on the invalidity of the formula occurs in

every period when $r_n = 0$. Thus, the IF estimation using eq. 3.12 has limitation in real situation.

In the case of linear chirp-type interference, Δf is not zero but a certain value. Thus, eq. 3.13 is not valid and has additional terms due to Δf .

$$\frac{r_{n+1}+r_{n-1}}{2r_n} = \frac{\cos\left(2\pi n\left(S_{t\_n}\right)+2\pi\frac{\Delta f}{2}\right)\cos\left(2\pi n\left(S_{t\_n}\right)+2\pi\frac{\Delta f}{2}n\right)}{2\cos\left(2\pi n\left(S_{t\_n}\right)\right)}$$
$$= \left[\cos\left(2\pi\frac{\Delta f}{2}\right) - tan\left(2\pi n\left(S_{t\_n}\right)\right)\sin\left(2\pi\frac{\Delta f}{2}\right)\right]\cos\left(2\pi S_{t\_n}+2\pi\frac{\Delta f}{2}n\right) \tag{3.13}$$

If Δf is a very small value, $\cos\left(2\pi\frac{\Delta f}{2}\right)=1$, $\sin\left(2\pi\frac{\Delta f}{2}\right)=\pi\Delta f$.

With these values, eq. 3.14 is rearranged as follows:

$$\frac{r_{n+1}+r_{n-1}}{2r_n} = \left[1-\left(\pi\Delta f\right)tan\left(2\pi n\left(S_{t\_n}\right)\right)\right]\cos\left(2\pi S_{t\_n}+2\pi\frac{\Delta f}{2}n\right)$$
$$= \left[1-\left(\pi\Delta f\right)tan\left(2\pi n\left(S_{t\_n}\right)\right)\right]\cos\left(2\pi f_n\right) \tag{3.14}$$

$$\therefore f_n = \frac{1}{2\pi}\cos^{-1}\left(\frac{1}{\left[1-\left(\pi\Delta f\right)tan\left(2\pi n\left(S_{t\_n}\right)\right)\right]}\frac{r_{n+1}+r_{n-1}}{2r_n}\right) \tag{3.15}$$

In eq. 3.15, the tangent term causes a calculation error when the phase reaches the $\frac{\pi}{2}(2n-1)$ period regardless of the measurement noise. If the measurement noise is calculated by eq. 3.15, an unexpected calculation error occurs throughout the interval, as shown in figure 3.3.

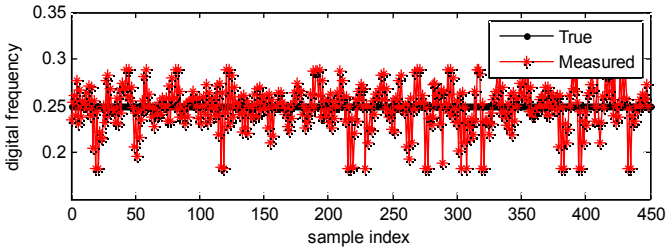

a) The measurement of the single-tone CWI (J/S 30dB)

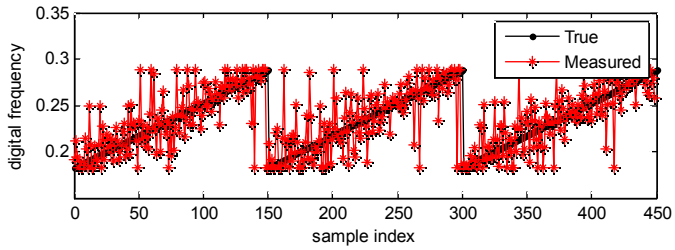

b) The measurement of the chirp-type interference (J/S 30dB)

Figure 3.3 The frequency measurement of the GNSS interference

In eq. 3.15, the three samples (r_{n-1}, r_n, r_{n+1}) are effected on the measurement noise in real situation and their probability density are expressed as

$$\begin{aligned} r_{n+1} &\approx N\left(m_{n+1}, \sigma^2\right) \\ r_n &\approx N\left(m_n, \sigma^2\right) \\ r_{n-1} &\approx N\left(m_{n-1}, \sigma^2\right) \end{aligned} \tag{3.16}$$

where three samples are Gaussian random variables and their means are m_{n-1}, m_n, m_{n+1}, respectively. It is assumed that variance of all samples is set to σ^2. Then, the mean and variance of $(r_{n+1} + r_{n-1}) / 2r_n$ is shown as

$$E\left[\frac{r_{n+1} + r_{n-1}}{2r_n}\right] = \frac{m_{n+1} + m_{n-1}}{2m_n} \tag{3.17}$$

$$\begin{aligned} \operatorname{var}\left[\frac{r_{n+1} + r_{n-1}}{2r_n}\right] &\approx \frac{\left(\operatorname{var}\left[r_{n+1}\right] + \operatorname{var}\left[r_{n-1}\right]\right)}{E\left[2r_n\right]^2} + \frac{\operatorname{var}\left[2r_n\right]\left(E\left[r_{n-1}\right] + E\left[r_{n+1}\right]\right)^2}{E\left[2r_n\right]^4} \\ &\approx \frac{1}{2}\left(\frac{\sigma}{m_n}\right)^2 + \frac{\sigma^2}{4}\left(\frac{m_{n-1} + m_{n+1}}{m_n^2}\right)^2 \end{aligned} \tag{3.18}$$

where three samples are independent each other and derivation of variance in eq. 3.18 is based on [16]. If $m_{n-1} = m_n - \Delta r,\ m_{n+1} = m_n + \Delta r,$ and $-1 < m_n < 1$, the variance in eq. 3.18 can be approximated as

$$\mathrm{var}\left[\frac{r_{n+1}+r_{n-1}}{2r_n}\right] \approx \frac{1}{2}\frac{\sigma^2}{m_n^2}+\frac{\sigma^2}{m_n^2}=\frac{3}{2}\frac{\sigma^2}{m_n^2}>1.5\sigma^2, \quad \left(\because \frac{1}{m_n^2}>1\right) \tag{3.19}$$

As shown in eq. 3.19, the variance of $(r_{n+1}+r_{n-1})/2r_n$ depends on the value of the received signal, m_n and its value is always bigger than $1.5\sigma^2$. Thus, it has a severe effect on the calculation results, which causes the unexpected calculation error.

In order to estimate the interference frequency correctly, the calculation error should be reduced and Δf should be tracked exactly. However, Δf is an unknown parameter and its value is different according to types of commercial jammer. Thus, for estimating and reducing the error, a model-based filtering method is needed. In this dissertation, an adaptive fading Kalman filter is used to reduce the error and track the interference frequency and Δf .

3.2.2 Adaptive Fading Kalman Filter

The concept of the adaptive fading Kalman filter centers on the application of a factor to the Kalman gain to adjust the tracking performance of the filter. In most adaptive fading Kalman filters [33, 34, 35], this factor is calculated according to the relationship between the calculated innovation covariance and the estimated innovation covariance, as the innovation covariance of the filter can present the effect of unaccounted errors [35]. The innovation covariance of the filter is determined by

$$C_n = \mathrm{E}\left[\left(z_n - \hat{z}_n^-\right)\left(z_n - \hat{z}_n^-\right)^T\right] = \mathbf{H}\mathbf{P}_n^-\mathbf{H}^T + \mathbf{R}_n \tag{3.20}$$

where C_n refers to the calculated innovation covariance and $\hat{z}_n^-$ is the estimated measurement, $\mathbf{H}\hat{\mathbf{x}}_n^-$. $\mathbf{H}$ is the measurement matrix, $\mathbf{P}_n^-$ is the prior predicted error covariance and $\mathbf{R}_n$ is the measurement noise covariance of the filter.

The estimated innovation covariance can be expressed by

$$\hat{C}_n = \frac{1}{M-1}\sum_{i=n-M+1}^{n}\left(z_i - \hat{z}_i^-\right)\left(z_i - \hat{z}_i^-\right)^T \tag{3.21}$$

where M is the window size. With eqs. 3.20 and 3.21, the factor which adjusts the Kalman gain is obtained, as follows:

$$\alpha_n = \max\left\{1, \frac{trace\left(\hat{C}_n\right)}{trace\left(C_n\right)}\right\} \tag{3.22}$$

The factor is used to offset the measurement error by decreasing the Kalman gain. The Kalman gain is reduced by

$$\mathbf{K}_n = \frac{1}{\alpha_n}\mathbf{P}_n^-\mathbf{H}^T\left[\mathbf{H}\mathbf{P}_n^-\mathbf{H}^T + \mathbf{R}_n\right]^{-1} \tag{3.23}$$

Under normal operation, α_n will be set to one because $trace\left(\hat{C}_n\right)$ is smaller than $trace(C_n)$ and the Kalman gain is updated using a general formula. If severe measurement error occurs, α_n exceeds 1. In such a case, the Kalman gain decreases by $1/\alpha_n$, allowing it to depend less on the measurement information.

The remaining filter equations are identical to those used for the conventional discrete Kalman filter [35].

$$\hat{\mathbf{x}}_n^- = \mathbf{F}\hat{\mathbf{x}}_{n-1}^+ \tag{3.24}$$

$$\mathbf{P}_n^- = \mathbf{F}\mathbf{P}_{n-1}^+\mathbf{F}^T + \mathbf{Q}_n \tag{3.25}$$

$$\mathbf{P}_n^+ = \left(\mathbf{I} - \mathbf{K}_n\mathbf{H}\right)\mathbf{P}_n^- \tag{3.26}$$

$$\hat{\mathbf{x}}_n^+ = \hat{\mathbf{x}}_n^- + \mathbf{K}_n \left(z_n - \mathbf{H}\hat{\mathbf{x}}_n^- \right) \tag{3.27}$$

Additionally, in order to improve the tracking performance of the interference frequency, two filter models are used according to the type of interference.

For the single-tone CWI, the system model of the Kalman filter is

$$\mathbf{x}_{n+1} = \mathbf{F}\mathbf{x}_n + \mathbf{w}_n \tag{3.28}$$

where the states are the frequency and variation of the frequency, which are expressed as $\mathbf{x}_n = \left[f_n, \Delta f_n \right]^T$. $\mathbf{F} = \begin{bmatrix} 1 & 1 \\ 0 & 1 \end{bmatrix}$ and, $\mathbf{w}_n = \begin{bmatrix} w_n \\ 0 \end{bmatrix}$ where $\mathbf{w}_n$ is the process noise, which is white Gaussian noise $\left(w_n \approx N\left(0,\ \sigma_w^2\right) \right)$. The proper state model of GNSS interference is selected according to the identification result of the interference from the proposed identification logic, which is explained in the next section.

The measurement model of the Kalman filter is

$$z_n = \mathbf{H}\mathbf{x}_n + v_n \tag{3.29}$$

where $\mathbf{H} = [1 \quad 0]$ and v_n is the measurement noise, whose distribution is $N\left(0,\ \sigma_v^2\right)$. The measurement model is applied to both types of interference and the proposed system is observable, as the rank of the observability matrix is full.

However, the state model of chirp-type interference is only satisfied when the sample index n is within the sweep period, as the frequency of chirp-type interference is f_0 at the beginning of every sweep period. In order to estimate the frequency of the interference accurately, it is necessary to reset the filter state f_n to f_0 when $n = T-1$. Here, f_0 is calculated using estimated states of the filter when $n = T-1$, nearly converging to the true values of f_n and Δf_n.

$$\begin{aligned}
\hat{f}_0 &= \hat{f}_{T-1} - (T-1)\Delta\hat{f}_{T-1} \\
&= \left(f_{T-1} + \tilde{f}_{T-1}\right) - (T-1)\left(\Delta f + \Delta\tilde{f}_{T-1}\right) \\
&= f_{T-1} - (T-1)\Delta f + \tilde{f}_{T-1} - (T-1)\Delta\tilde{f}_{T-1} \\
&= f_0 + \tilde{f}_{T-1} - (T-1)\Delta\tilde{f}_{T-1} = f_0 + \tilde{f}_0
\end{aligned} \tag{3.30}$$

where $\hat{f}_0$ is the estimation of f_0 which is an unknown value depending on the property of the received interference. $\hat{f}_n$ and $\Delta\hat{f}_n$ are estimated states. Estimation errors refer to $\tilde{f}_n$ and $\Delta\tilde{f}_n$.

The initial error covariance, $\mathbf{P}_{0\_T}(1,1)$ of the filter is also reinitialized at the beginning of the sweep period. $\mathbf{P}_{0\_T}(1,1)$ is expressed by

$$\begin{aligned}\mathbf{P}_{0\_T}(1,1) &= E\left[\left(f_0 - \hat{f}_0\right)^2\right] \\ &= E\left[\left(\tilde{f}_{T-1} - (T-1)\Delta\tilde{f}_{T-1}\right)^2\right] \\ &= E\left[\tilde{f}_{T-1}^2\right] + (T-1)^2 E\left[\Delta\tilde{f}_{T-1}{}^2\right] \\ &\approx \mathbf{P}_{T-1}^{+}(1,1) + (T-1)^2 \mathbf{P}_{T-1}^{+}(2,2)\end{aligned} \tag{3.31}$$

In this equation, $\tilde{f}_n$ and $\Delta\tilde{f}_n$ are uncorrelated and $\mathbf{P}_{T-1}^{+}$ is the posterior predicted error covariance.

3.2.3 Sweep Period Estimation by Pattern Recognition

The sweep period of the interference only exists in case of chirp-type interference, and it is used to reset the filter state and initial error covariance to track the chirp-type interference. To estimate the sweep period the measurement passing through LPD [36] is normalized and expressed as

$$z_{G\_n} = \gamma z_{G\_(n-1)} - (1-\gamma)\left(\frac{z_n - z_{n-6}}{\lambda_z}\right) \tag{3.32}$$

where γ is the forgetting factor and λ_z is the normalization factor, which refers to $\beta \times \left({(f_{\max} - f_{\min})}/{f_s} \right)$ and is a design parameter to enhance the peak pattern. β is the scale factor, and $f_{\min}$ and $f_{\max}$ are respectively the minimum and maximum frequency of observable frequency bandwidth. z_{G_n} is a combination of a low-pass filter and differentiator. $z_n - z_{n-6}$ is the main term and represents the simple differentiator which is used to calculate the change rate between the past data and the present data. When z_n changes dramatically in the end of sweep period, differentiator converts the change of frequency into a peak as shown in figure 3.4.

This filter has very simple structure for increasing the tracking speed of filter. The transfer function of LPD [36] is shown below.

$$G(z) = 1 - z^{-6} \tag{3.33}$$

Figure 3.4 shows the value of z_{G_n} when chirp-type interference whose J/S is 30dB is received. In this case, z_{G_n} has a peak at the beginning of the sweep period where the frequency of the interference changes radically. If the time index at the peak is measured, the sweep period can be estimated. In the case of the single-tone CWI, the peak does not exist because there is no frequency change in the single-tone CWI.

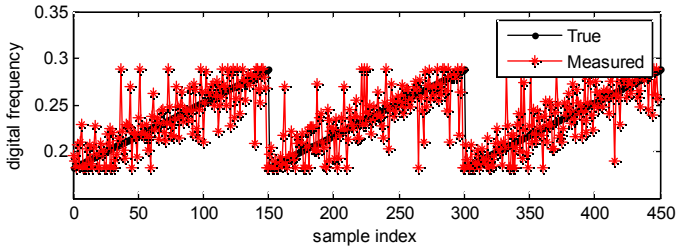

a) Frequency of the chirp-type interference

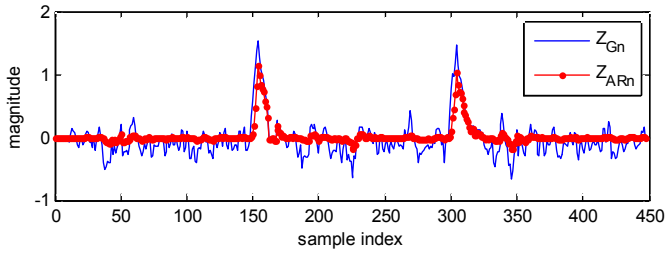

b) Results of period estimation

Figure 3.4 The period estimation results in the case of chirp-type interference

The value of z_{G_n} when the single-tone CWI is received is shown in figure 3.5. According to the difference between the single-tone CWI and the chirp-type interference, it is possible to distinguish between the two types. However, the peak of z_{G_n} cannot easily be recognized by a certain threshold because z_{G_n} has a considerable amount of noise due to the measurement error of z_n

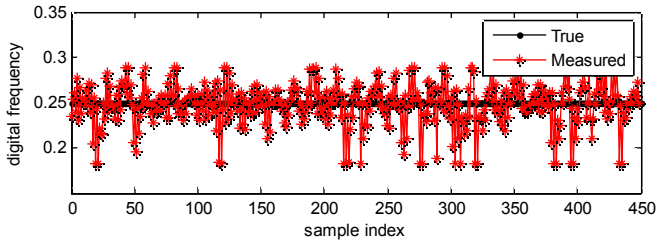

a) Frequency of the single-tone CWI

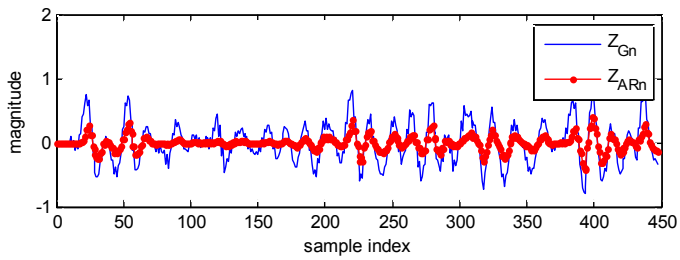

b) Results of period estimation

Figure 3.5 The period estimation results in case of single-tone CWI

A pattern enhancement algorithm [37, 38, 39] is used to detect the peak effectively so as to reduce the effect of the noise. This algorithm is based on an autoregressive (AR) model, and the AR coefficients are estimated using a Kalman filter. In addition, z_{G_n} is described by an AR model, and the model is given as

$$z_{G\_n} = \sum_{i=1}^{p} \gamma_{i\_n} z_{G\_(n-i)} + v_{AR\_n} \tag{3.34}$$

where p is the order of the model, which is set to 5 to obtain a noiseless pattern and to consider the computation load; γ_{i_i} is the AR coefficient; and v_{AR_n} is the white Gaussian noise with a zero mean and variance of σ_{AR}^2. To estimate the AR coefficient, the state and measurement models of the Kalman filter are

$$\mathbf{\Gamma}_n = \mathbf{A}\mathbf{\Gamma}_{n-1} + \boldsymbol{\omega}_n \tag{3.35}$$

$$z_{G\_n} = \mathbf{E}_n^T \mathbf{\Gamma}_n + v_{AR\_n} \tag{3.36}$$

where $\mathbf{\Gamma}_n = \left[\gamma_{1\_n}, \dots, \gamma_{p\_n}\right]^T$, $\mathbf{A} = diag(0.2, \cdots 0.2)$ which is a diagonal matrix and a dimension is $p \times p$. The matrix A reflects the correlation of the coefficients between different time instants. It is assumed that there is no correlation between the coefficients in time index n with those in time index $n-1$. Thus,

the diagonal elements of A are set to a value that is less than one. $\mathbf{E}_n = \left[z_{G\_(n-1)}, \cdots, z_{G\_(n-p)} \right]^T$, $\boldsymbol{\omega}_n$ is white Gaussian noise with a zero mean and covariance of $\mathbf{Q}_{AR}$. As a result, the enhancement pattern of z_{G_n} can be expressed by

$$z_{AR\_n} = \mathbf{E}_n^T \hat{\boldsymbol{\Gamma}}_n \tag{3.37}$$

where $\hat{\boldsymbol{\Gamma}}_n$ is the AR coefficient estimated by the Kalman filter and z_{AR_n} is shown in the lower part of figures 3.4 and 3.5. The peak of z_{AR_n} is detected according to the maximum value above the selected threshold, which is set to $\beta_{en} \times \left({(f_{\max} - f_{\min})}/{f_s} \right)$, with β_{en} being the enhancement rate. Consequently, the estimated time index at the peak is sent to the filter and used to reset the filter, after which this is applied to generate the pulsed signal to identify the type of interference received.

3.2.4 Interference Identification Logic

The proposed interference identification logic is based on the unique pattern of z_{G_n}. As mentioned in the previous section, peaks of z_{G_n} is only generated if chirp-type interference is received. As a result, the type of interference can be determined according to the characteristic of z_{AR_n}, which is an enhancement value of z_{G_n}. It is assumed that the types of interference received are limited to single-tone CWI and chirp-type interference, which are the most extensively used in a commercial jammer. In addition, it is assumed that the existence of interference in the received signal is already known considering the results of previous work [11], which uses the property of the AGC gain. The interference is the main source that changes the AGC gain because the power of the GNSS signal is below the thermal noise floor. Thus, AGC can be a valuable tool for detecting interference [40, 41]. The value of the AGC gain was examined according to the increase in the power of the interference in previous work [2, 3]. Based on these results, the value of the AGC gain is also used to detect the existence of interference sources in this dissertation. If the magnitude of the AGC gain is below a certain threshold, implying that an interference signal exists in the received signal, the proposed tracking algorithm is activated to track its frequency.

Initially in the interference identification logic, the pulsed signal is generated as follows:

$$S_{P\_n} = \begin{cases} 1, & z_{AR\_n} > \gamma_{en} \times \left({(f_{\max} - f_{\min})}/{f_s} \right) \\ 0, & z_{AR\_n} \le \gamma_{en} \times \left({(f_{\max} - f_{\min})}/{f_s} \right) \end{cases} \tag{3.38}$$

Here, S_{P_n} is the pulsed signal calculated from z_{AR_n} using the threshold. This result is shown in figure 3.6. Secondly, a sliding-window sum algorithm is employed to accumulate the S_{P_n} in order to set the detection parameter, S_{c_n}.

$$S_{c\_n} = \sum_{i=n-M_T}^{n} S_{P\_i} \quad , \; n \ge M_T \tag{3.39}$$

In this equation, M_T denotes the window size, which is set to 150 here. It is designed to detect chirp-type interference whose sweep rate exceeds 1×10^{12} MHz. The results of S_{c_n} are shown in figure 3.7. If chirp-type interference is received, the value of S_{P_n} is generated by eq. 3.38 such that S_{c_n} increases. As a result, the received interference can be identified as long as the threshold is carefully selected.

$$S_{ID\_n} = \begin{cases} 1, & S_{c\_n} \le 2\% \ of \ M_T \\ 2, & S_{c\_n} > 2\% \ of \ M_T \end{cases} \tag{3.40}$$

In these equations, $S_{ID\_n} = 1$ refers to single-tone CWI and $S_{ID\_n} = 2$ refers to chirp-type interference. The threshold is set to 2% of the window size, as selected according to the width of the pulse of S_{P_n} , which is determined by the threshold in eq. 3.38. The threshold in eqs. 3.38 and 3.40 is set to detect chirp-type interference whose J/S value exceeds 30dB. The proposed interference identification logic works well, as shown in figure 3.8.

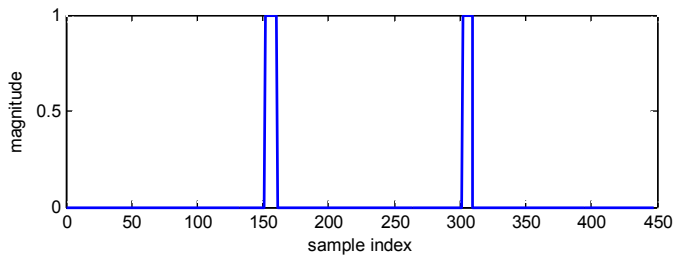

Figure 3.6 The results of S_{P_n} with chirp-type interference

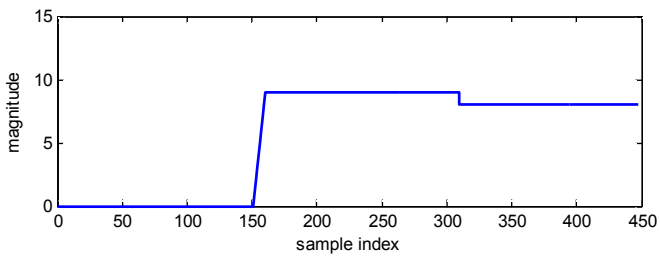

Figure 3.7 The results of S_{c_n} with chirp-type interference

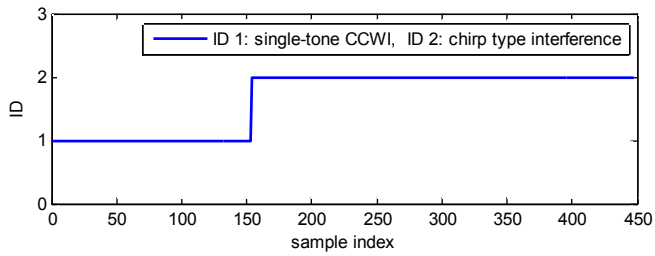

Figure 3.8 The identification result with chirp-type interference

In order to verify its performance, a Monte Carlo simulation is conducted when chirp-type interference with a J/S value of 30dB is added to a GNSS signal. However, a delay of the identification which is equal to M_T occurs, as shown in figures 3.7 and 3.8, due to the sliding-window sum algorithm, which accumulates S_{P_n} according to the moving window. This delay causes some degree of estimation error in the tracking algorithm, but this can be overridden because its value is too small to affect the frequency tracking algorithm severely. The detection probability is been also calculated by Monte Carlo simulations on the basis of 100 independent runs in the proposed method when chirp-type interference exists in the received signal at every 2dB of J/S.

The detection probability is defined as follows:

$$P = \frac{N_p}{N_s} \tag{3.41}$$

Here, the numerator refers to the number of correct chirp-type interference detection instances and the denominator refers to the number of iterations. Figure 3.9 refers to the probability of recognizing the chirp-type interference pattern according to J/S. As shown in this figure, the proposed method can identify chirp-type interference perfectly even when the J/S exceeds 30 dB

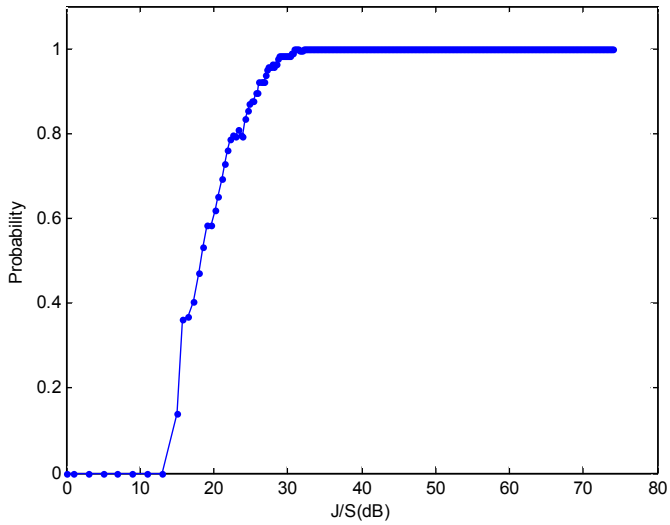

Figure 3.9 The detection probability of pattern recognition

3.2.5 Simulations and Analysis

The performance of the proposed algorithm is verified in two simulations. In the first simulation, the frequency tracking performance is compared to other methods, in this case a conventional discrete Kalman filter (DKF) and an adaptive fading filter without period estimation (AKF), whose models are identical to that shown in eq.3.28 and 3.29. In the AKF case [35], the prior predicted error covariance and the Kalman gain are increased by α_n, as follows:

$$\mathbf{P}_n^- = \alpha_n \left(\mathbf{F}\mathbf{P}_{n-1}^+ \mathbf{F}^T + \mathbf{Q}_n \right) \tag{3.42}$$

$$\mathbf{K}_n = \alpha_n \mathbf{P}_n^- \mathbf{H}^T \left[\mathbf{H}\mathbf{P}_n^- \mathbf{H}^T + \mathbf{R}_n \right]^{-1} \tag{3.43}$$

The increase in the Kalman gain implies greater dependence on the measurement information and consequently increases the sensitivity of the response to frequency changes. Thus, the filter can track chirp-type interference except when it is used with the proposed sweep period estimation method. Only the chirp-type interference is received and the identification logic is not applied to this simulation in order to compare only the frequency tracking performance. The signal power of the received GNSS signal is -130dBm, the overall noise floor is set to -114dB/MHz, and the J/S is 30dB.

In the second simulation, the frequency tracking and interference identification performance levels are verified. The single-tone CWI is

received initially and 300 samples later, after which the chirp-type interference is received, as shown in figure 3.10. The intermediate frequency of the single-tone CWI is set to 0.25 in digital frequency and the remaining settings are identical to those in the first simulation.

Tracking results of the two scenarios are shown in figures 3.11 and 3.12.

In figure 3.11, the DKF tracks the interference frequency well in the first period, but the tracking error increases after the first period because the convergence speed of the filter is slower than the rate of change of the frequency near the beginning of the period. In the AKF case, the convergence rate of the filter is improved by increasing the Kalman gain and prior predicted error covariance, reducing the tracking error relative to that of the DKF case. However, increasing the Kalman gain also leads to estimation error due to the overdependence on the measurement, which has a considerable amount of noise, as shown in figure 3.3. Comparing the frequency estimation results, the proposed algorithm demonstrates better tracking performance than the DKF and AKF methods, as the proposed algorithm resets the filter at the beginning of the sweep period by means of period estimation. The frequency estimation RMSE of the proposed algorithm is 0.0071, that of the DKF method is 0.0220, and that with the AKF is 0.0115. When the sampling frequency is set to 38.192 MHz, the RMSE becomes 270 KHz, 840 KHz and 439 KHz, respectively. As shown in the results, the only proposed tracking algorithm satisfies the mitigation condition.

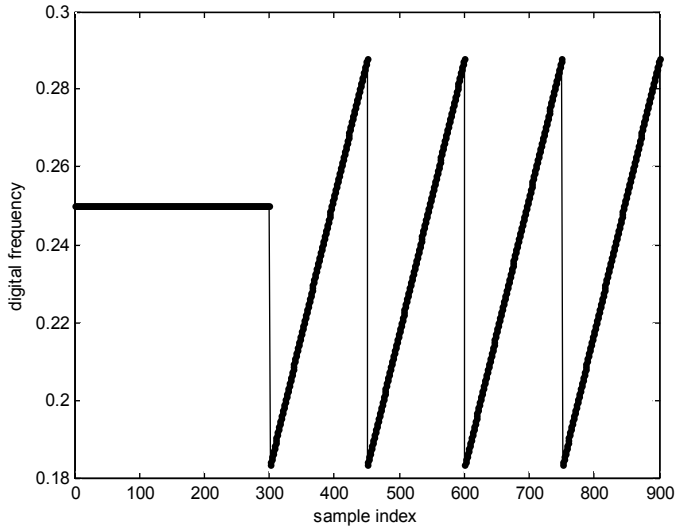

Figure 3.10 The scenario of the second simulation

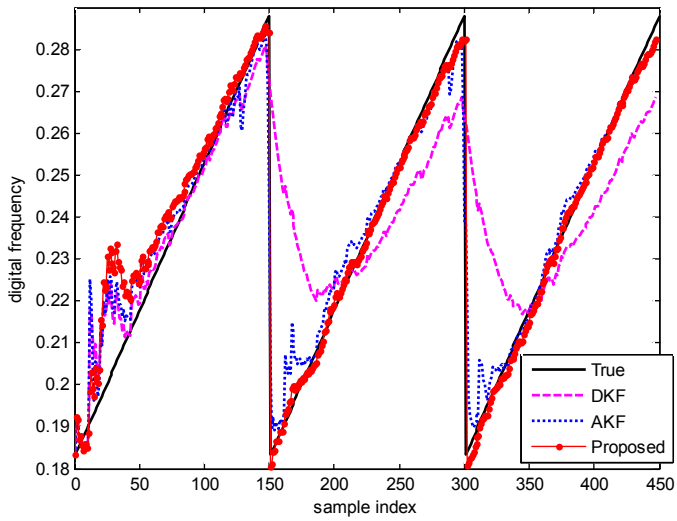

Figure 3.11 The frequency tracking results of the first simulation

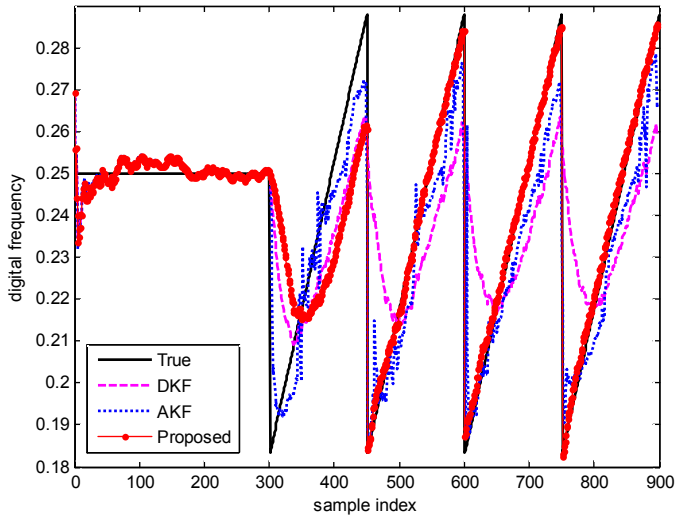

Figure 3.12 The frequency tracking results of the second simulation

In figure 3.12, the results of the second simulation are presented. The DKF has estimation error in the period of the first 300 samples due to the use of an improper filter model, which adds an error of Δf to the estimated frequency value. During the rest of the period, its performance is identical to that of the first simulation. In the AKF case, the adaptive structure leads to estimation error throughout the period due to the relatively high level of dependence on z_n, whereas the proposed algorithm with a proper filter model selected by the identification result estimates the frequency of the interference relatively well. However, the proposed algorithm produces estimation error upon a change in the type of interference due to the delay of the identification logic, which is caused by the sliding window sum algorithm, as mentioned

earlier. Likewise, the estimation error can be ignored because the sampling rate is set to 38.192 MHz such that the period during which the error occurred is very short.

As shown in figures 3.12 and 3.13, which presents the estimation result of Δf . 450 samples later, the proposed algorithm estimates f and Δf accurately by utilizing the proper filter models according to the type of interference and the reinitialization of the filter parameter at the beginning of the sweep period when the chirp-type interference is received.

Figures 3.14, 3.15, 3.16, and 3.17 show each step of the identification logic. Figure 3.14 presents the pattern recognition outcome with LPD and the enhancement result of the second simulation. Peaks are only generated when chirp-type interference is received. In addition, S_{P_n} , S_{c_n} and the identification result of the second simulation are presented in the rest of the figure. As shown in these figures, the proposed identification logic works well.

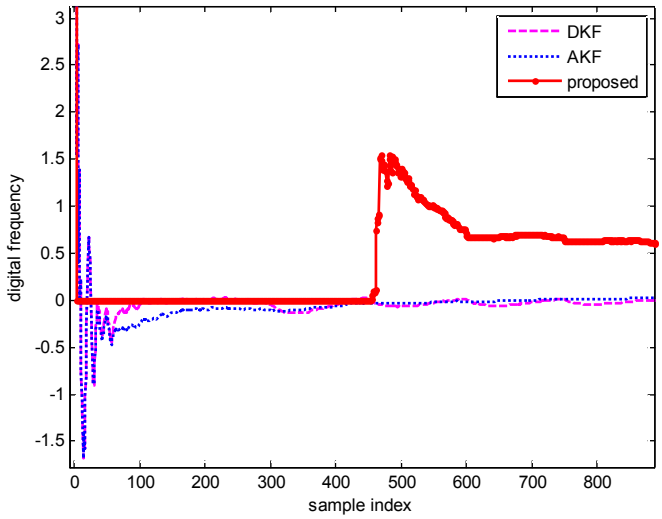

Figure 3.13 The estimation results of the variation of the frequency in the second simulation (y-axis unit: 1×10^{-3})

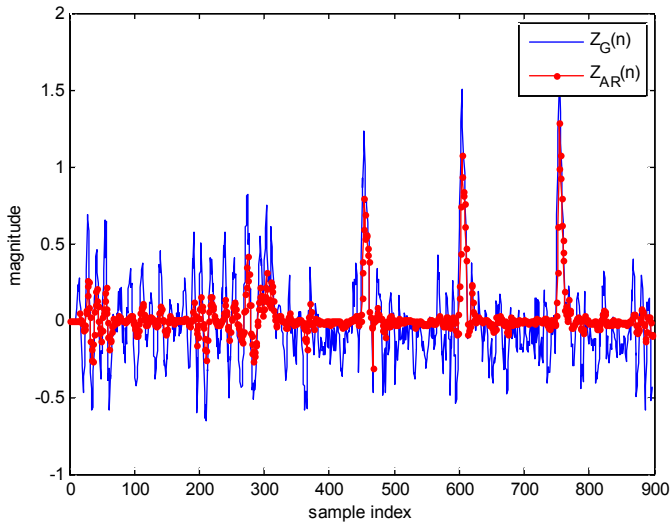

Figure 3.14 The pattern recognition and enhancement results of the second simulation

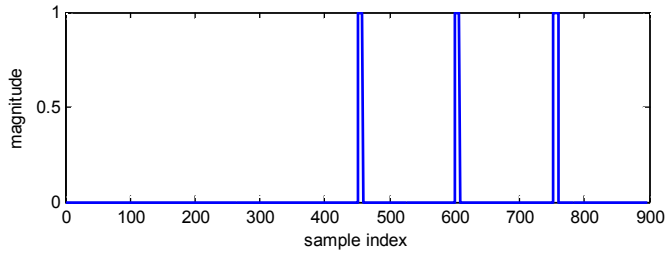

Figure 3.15 The results of S_{P_n} in the second simulation

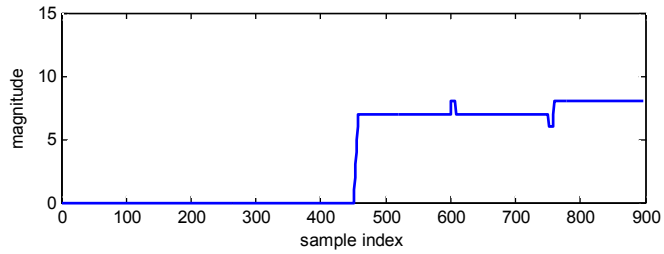

Figure 3.16 The results of S_{c_n} in the second simulation

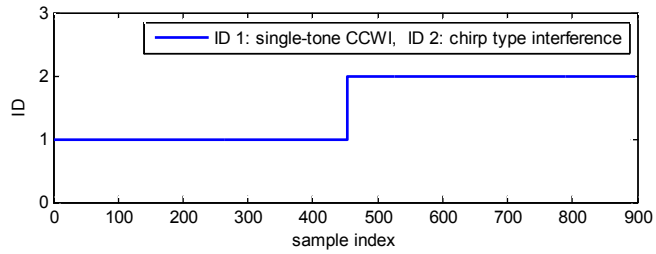

Figure 3.17 The identification result in the second simulation

The algorithm can only track linear chirp-type interference which has a dramatic change at the end of sweep period due to the limited performance of LPD which is used to estimate the sweep period of the interference. If another chirp-type which does not have the dramatic change at the end of sweep period is received, the LPD cannot recognize the sweep period of the different chirp-type interference. Furthermore, as a constant rate of frequency change model is used, a frequency tracking error may occur when the frequency change rate is not constant in the sweep period. In order to deal with these problems, the revised frequency tracking algorithm which does not depend on estimating the sweep period is needed, to track the various chirp-type interferences. And a nonlinear frequency-tracking model is also needed to reduce the tracking error.

3.3 An Adaptive Kalman Filter Based Method with Fourier Series

The chirp-type frequency model explained in the previous section is only valid within the boundary T . Hence, an extra algorithm that estimates the boundary should be needed to use the above frequency model in the next period [28]. However, if the Fourier series based frequency model is used, the extra algorithm is not needed to track frequency [42]. The new frequency model designed by the Fourier series is expressed as

$$\begin{aligned} f_m(n) &= a_0 + a_1\cos(wn) + b_1\sin(wn) + \cdots \\ &\quad + a_N\cos(Nwn) + b_N\sin(Nwn) \\ &= \sum_{i=0}^{N}\{a_i\cos(iwn) + b_i\sin(iwn)\} \end{aligned} \tag{3.44}$$

where N is the order of the Fourier series. a_i and b_i are coefficients of the cosine and sine terms, respectively. w is a frequency of the periodic signal.

In this section, the proposed frequency tracking algorithm for chirp-type interference detection is introduced. The main feature of chirp-type interference is that its frequency changes periodically. In the previous work, we only considered a linear chirp-type model whose frequency increases linearly within the one period and is reinitialized at the beginning of every period. In general, according to [18], most types of chirp interference are linear types. However, some jammers use nonlinear chirps instead [43].

Thus, we are focusing on tracking various chirp-type interferences regardless of the form of the frequency change in period T and the modeling is with the Fourier series. Properly estimating the Fourier series' coefficients is very important for tracking the time varying periodic signal. Most of the existing methods use batch processing, such as a nonlinear least-square curve fitting. However, in order to track a time-varying signal in real time, a sequential processing based method is needed and one of the methods is a Kalman filter-based method. The first Kalman filter-based method is proposed in [44]. This paper shows that all harmonic components of a signal measured with noise can be estimated by the Kalman filter when the period of the signal is known. However, in real situations, the period of the signal is unknown or varying in most case according to the communication characteristics. Hence, a modified system model of state variables is needed to estimate the period and track the signal. In addition, a modified adaptive fading logic is also required in the Kalman filter in order to maintain signal tracking performance when measurement error occurs.

3.3.1 State Variables and Filter Models

The proposed system is governed by continuous-time dynamics whereas the measurement is obtained at discrete instants of time. In order to estimate the coefficients of the Fourier series, a hybrid extended Kalman filter (HEKF) is used [45]. The HEKF considers systems with continuous-time dynamics and discrete-time measurements. States variables are components of the Fourier series [44] and if the fifth-order Fourier series are considered, state variables are expressed as

$$\mathbf{x}=\begin{bmatrix} x_1 \\ x_2 \\ x_3 \\ x_4 \\ x_5 \\ x_6 \\ x_7 \\ x_8 \\ x_9 \\ x_{10} \\ x_{11} \end{bmatrix}=\begin{bmatrix} \omega \\ a_1\cos(\omega t)+b_1\sin(\omega t) \\ -a_1\sin(\omega t)+b_1\cos(\omega t) \\ a_2\cos(2\omega t)+b_2\sin(2\omega t) \\ -a_2\sin(2\omega t)+b_2\cos(2\omega t) \\ a_3\cos(3\omega t)+b_3\sin(3\omega t) \\ -a_3\sin(3\omega t)+b_3\cos(3\omega t) \\ a_4\cos(4\omega t)+b_4\sin(4\omega t) \\ -a_4\sin(4\omega t)+b_4\cos(4\omega t) \\ a_5\cos(5\omega t)+b_5\sin(5\omega t) \\ -a_5\sin(5\omega t)+b_5\cos(5\omega t) \end{bmatrix} \tag{3.45}$$

The proposed system equation with continuous-time dynamics and discrete-time measurements are given as follows:

$$\dot{\mathbf{x}} = \begin{bmatrix} \dot{x}_1 \\ \dot{x}_2 \\ \dot{x}_3 \\ \dot{x}_4 \\ \dot{x}_5 \\ \dot{x}_6 \\ \dot{x}_7 \\ \dot{x}_8 \\ \dot{x}_9 \\ \dot{x}_{10} \\ \dot{x}_{11} \end{bmatrix} = \underbrace{\begin{bmatrix} 0 \\ x_1 x_3 \\ -x_1 x_2 \\ x_1 x_5 \\ -x_1 x_4 \\ x_1 x_7 \\ -x_1 x_6 \\ x_1 x_9 \\ -x_1 x_8 \\ x_1 x_{11} \\ -x_1 x_{10} \end{bmatrix}}_{f(\mathbf{x},t)} + \mathbf{w}(t) \tag{3.46}$$

$$\begin{aligned} y_n &= f_n = a_0 + x_2 + x_4 + x_6 + x_8 + x_{10} + v_n \\ &= a_0 + \mathbf{H}_n \mathbf{x}_n + v_n \end{aligned} \tag{3.47}$$

Where $\mathbf{w}(t)$ is continuous-time white noise with covariance $\mathbf{Q}$ and v_n is discrete-time white noise with variance R_n. y_n refers to the frequency measurement. In proposed algorithm, the measurement is obtained by eq. 3.12 from the received signal written in eq. 2.1. a_0 is a given variable which is obtained as $\frac{1}{N}\sum_{n=1}^{N} y_n$. N is the total number of data samples. $\mathbf{H}_n$ is a 1×11 matrix and $\mathbf{H}_n = [01010101010]$. These models can be extended according to

the order of the Fourier series. If users select an M th order Fourier series, the total number of states variables is $2M+1$, which will have an extended form similar to that of eq. 3.45.

For increasing a discrete time step n, perform the following procedures [45]. Integrate the state estimate and its covariance from time $n-1$ to n^- (before n step measurement update) as follows:

$$\dot{\hat{\mathbf{x}}} = f\left(\hat{\mathbf{x}}, t\right) \tag{3.48}$$

$$\dot{\mathbf{P}} = \mathbf{F}\mathbf{P} + \mathbf{P}\mathbf{F}^T + \mathbf{Q} \tag{3.49}$$

where $\mathbf{F} = \left.\frac{\partial f}{\partial \mathbf{x}}\right|_{\hat{\mathbf{x}}}$. At the end of this integration, $\hat{\mathbf{x}} = \hat{\mathbf{x}}_k^-$ and $\mathbf{P} = \mathbf{P}_k^-$ are obtained.

At time n, incorporate the measurement y_n into the state estimate and estimation covariance as follows (measurement update):

$$\mathbf{K}_n = \mathbf{P}_n^- \mathbf{H}_n^T \left(\mathbf{H}_n \mathbf{P}_n^- \mathbf{H}_n^T + R_n\right)^{-1} \tag{3.50}$$

$$\hat{\mathbf{x}}_n^+ = \hat{\mathbf{x}}_n^- + \mathbf{K}_n \left(y_n - \mathbf{H}\hat{\mathbf{x}}_n^-\right) \tag{3.51}$$

$$\mathbf{P}_n^+ = \left(\mathbf{I} - \mathbf{K}_n \mathbf{H}_n\right) \mathbf{P}_n^- \left(\mathbf{I} - \mathbf{K}_n \mathbf{H}_n\right)^T + \mathbf{K}_n R_n \mathbf{K}_n^T \tag{3.52}$$

3.3.2 Filtering Error Analysis and Correction

In time update sequence of the hybrid Kalman filter, the numerical integration of $\hat{\mathbf{x}}_n^-$ causes the calculation error. If the rectangular integration is used, time update of states can be

$$\hat{\mathbf{x}}_n^- = \hat{\mathbf{x}}_{n-1}^+ + \dot{\hat{\mathbf{x}}} T_s \tag{3.53}$$

where $\hat{\mathbf{x}}_{n-1}^+$ refers to $n-1$th estimate result with measurement update and T_s is the sampling time. If a second state update is only considered in order to derive the equation easily, $\hat{x}_n^-$ term is expressed as

$$\begin{aligned}\hat{x}_n^- &= \underbrace{a_1 \cos\left(\omega\left(n-1\right)\right) + b_1 \sin\left(\omega\left(n-1\right)\right)}_{\hat{x}_{n-1}^+} \\ &\quad + \underbrace{\omega\left(-a_1 \sin\left(\omega n\right) + b_1 \cos\left(\omega n\right)\right)}_{\dot{\hat{x}}} \bullet T_s\end{aligned} \tag{3.54}$$

$$\begin{aligned}&= a_1\left(\cos\left(\omega n\right)\cos\omega - \sin\left(\omega n\right)\sin\omega\right) \\ &\quad + b_1\left(\sin\left(\omega n\right)\cos\omega + \cos\left(\omega n\right)\sin\omega\right) \\ &\quad + \omega T_s b_1 \cos\left(\omega n\right) - \omega T_s a_1 \sin\left(\omega n\right)\end{aligned} \tag{3.55}$$

If ω is small, $\cos\omega = 1$ and $\sin\omega = \omega.$ The above equation can be rearranged as

$$\hat{x}_n^- = a_1\cos(\omega n) + b_1\sin(\omega n) + \omega T_s b_1\cos(\omega n) - \omega T_s a_1\sin(\omega n)$$
$$= x_n^- + \sqrt{a_1^2 + b_1^2}\,\omega(1+T_s)\sin(\omega n + \delta\phi_1) \tag{3.56}$$

where x_n^- is true state update term in n th step and other term is an integration error. $\delta\phi_1$ is $Tan^{-1}(b_1/a_1)$. the integration error term is periodic and depends on coefficients and frequency of states. For example, the integration error of the tenth state in eq. 3.45 is $\sqrt{a_5^2 + b_5^2}\,5\omega(1+T_s)\sin(5\omega n + \delta\phi_5)$. The integration error effects on the state estimate value, which causes drift error in long term period.

In order to reduce the error effect on the state estimate, states and error covariance are initialized in every desired period. Initialization is performed as

$$\hat{\mathbf{x}}_n^- = \mathbf{x}\,|_{\hat{\mu}_{n-1}} = \begin{bmatrix} \hat{\omega} \\ \hat{a}_1 \cos(\hat{\omega} n) + \hat{b}_1 \sin(\hat{\omega} n) \\ -\hat{a}_1 \sin(\hat{\omega} n) + \hat{b}_1 \cos(\hat{\omega} n) \\ \hat{a}_2 \cos(2\hat{\omega} n) + \hat{b}_2 \sin(2\hat{\omega} n) \\ -\hat{a}_2 \sin(2\hat{\omega} n) + \hat{b}_2 \cos(2\hat{\omega} n) \\ \hat{a}_3 \cos(3\hat{\omega} n) + \hat{b}_3 \sin(3\hat{\omega} n) \\ -\hat{a}_3 \sin(3\hat{\omega} n) + \hat{b}_3 \cos(3\hat{\omega} n) \\ \hat{a}_4 \cos(4\hat{\omega} n) + \hat{b}_4 \sin(4\hat{\omega} n) \\ -\hat{a}_4 \sin(4\hat{\omega} n) + \hat{b}_4 \cos(4\hat{\omega} n) \\ \hat{a}_5 \cos(5\hat{\omega} n) + \hat{b}_5 \sin(5\hat{\omega} n) \\ -\hat{a}_5 \sin(5\hat{\omega} n) + \hat{b}_5 \cos(5\hat{\omega} n) \end{bmatrix} \tag{3.57}$$

$$\mathbf{P}_n^- = \mathbf{P}_{n-1}^+ \tag{3.58}$$

where $\hat{\mu}_{n-1}$ is the estimate parameters obtained from $n-1$ th estimate results.

The estimate parameters are coefficients (a, b) and frequency of each filter state.

$$\hat{\omega} = \hat{x}^{+}_{1,n-1} \tag{3.59}$$

$$\begin{bmatrix} \hat{a}_m \\ \hat{b}_m \end{bmatrix} = \begin{bmatrix} \cos\left(\left(m\hat{\omega}\right)\left(n-1\right)\right) & \sin\left(\left(m\hat{\omega}\right)\left(n-1\right)\right) \\ -\sin\left(\left(m\hat{\omega}\right)\left(n-1\right)\right) & \cos\left(\left(m\hat{\omega}\right)\left(n-1\right)\right) \end{bmatrix}^{-1} \begin{bmatrix} \hat{x}^{+}_{2\mathrm{m},n-1} \\ \hat{x}^{+}_{2\mathrm{m}+1,n-1} \end{bmatrix} \tag{3.60}$$

where $m = 1,2,...,5$. $\mathbf{P}_n^-$ has the same value of $n-1$ th error covariance because $\hat{\mathbf{x}}_n^-$ consists of $\hat{\mu}_{n-1}$ obtained from $n-1$ th state estimate result. The initialization period is set to one fourth of tenth state's integration error period ($\pi / 10\omega$) in order to prevent the integration error term reaches maximum value.

3.3.3 Stability of the Proposed Filter Model

In this section, the error behaviour of the proposed filter model is analyzed. In particular, it is shown that the proposed filter can converge on a minimum error value in few steps if the system satisfies the nonlinear observability rank condition and the initial estimation error as well as the disturbing noise terms are small enough [46]. Definitions and theorems proposed in [47, 48, 49, 50, 51] are used to analyze the convergence of the filter.

There are positive real numbers $\bar{a}, \bar{c}, \underline{p}, \bar{p}, \underline{q}, \underline{r}$ such that the following bounds on various matrices are fulfilled for every n:

$$\|\mathbf{F}_n\| \le \bar{a}\ , \quad \|\mathbf{H}_n\| \le \bar{c} \tag{3.61}$$

$$\underline{p}\mathbf{I} \le \mathbf{P}_n \le \bar{p}\mathbf{I} \tag{3.62}$$

$$\underline{q}\mathbf{I} \le \mathbf{Q}_n\ , \quad \underline{r}\mathbf{I} \le \mathbf{R}_n \tag{3.63}$$

where $\|\bullet\|$ denotes the Euclidian norm. The initial estimation error, $\boldsymbol{\delta}\mathbf{x}_0$ and nth estimation error, $\boldsymbol{\delta}\mathbf{x}_n$ satisfy

$$\underline{\varepsilon} \le \|\boldsymbol{\delta}\mathbf{x}_0\| \le \bar{\varepsilon}\ , \quad \|\boldsymbol{\delta}\mathbf{x}_n\| \le \bar{\varepsilon} \tag{3.64}$$

Finally, the expected value of estimation error is exponentially bounded in

$$E\{\|\boldsymbol{\delta}\mathbf{x}_n\|^2\} \le \frac{\overline{p}}{\underline{p}} E\{\|\boldsymbol{\delta}\mathbf{x}_0\|^2\}(1-\tau)^n + \frac{\underline{\varepsilon}^2}{2} \tag{3.65}$$

where, $(1-\tau)$ denotes $1/\left(1+\frac{\underline{q}}{\overline{p}\left(\overline{a}+\overline{ap}\left(\overline{c}^2\right)/\underline{r}\right)^2}\right)$ according to the inequality written in [46]. Real values of $\overline{a}, \overline{c}, \underline{p}, \overline{p}, \underline{q}, \underline{r}$ are set as follows.

If $a_m, b_m \le 0.01$ and $\omega_n^+ \le 0.05$,

$$\begin{aligned}\|\mathbf{F}_n\| &= \sqrt{x_4^2 + x_3^2 + 4\left(x_6^2 + x_5^2\right) + 9\left(x_8^2 + x_7^2\right) + 28x_2^2} \\ &= \sqrt{2\left(a_1^2 + b_1^2\right) + 8\left(a_2^2 + b_2^2\right) + 18\left(a_3^2 + b_3^2\right) + 28\left(\omega_n^+\right)^2} \\ &\le 0.264 = \overline{a}\end{aligned} \tag{3.66}$$

$$\|\mathbf{H}_n\| = \sqrt{1+1+1+1+1} = \sqrt{5} = \overline{c} \tag{3.67}$$

Other parameters are set to $\underline{p} = \underline{\varepsilon}^2$, $\overline{p} = \overline{\varepsilon}^2$, $\underline{q} = 1\times10^{-4}$ and $\underline{r} = 1\times10^{-3}$. The error bound is $[\underline{\varepsilon}, \overline{\varepsilon}] = [0.001, 0.01]$.

These values are substituted into eq. and $E\{\|\boldsymbol{\delta}\mathbf{x}_n\|^2\}$ becomes as

$$E\{\|\boldsymbol{\delta}\mathbf{x}_n\|^2\} < 100 \times \bar{\varepsilon}^2 \left(0.136\right)^n + 0.5\underline{\varepsilon}^2$$

$$< \left(1 \times 10^4 \left(0.136\right)^n + 0.5\right)\underline{\varepsilon}^2 \tag{3.68}$$

where $E\{\|\boldsymbol{\delta}\mathbf{x}_0\|^2\} = \bar{\varepsilon}^2$ and $\bar{\varepsilon} = 10\underline{\varepsilon}$. It is conformed that $E\{\|\boldsymbol{\delta}\mathbf{x}_n\|^2\}$ converges to $\underline{\varepsilon}^2$ in five steps according to the above equation $\left(n = \log(0.5/10^4)/\log(0.136) \approx 4.9\right)$ and its result is shown in figure 3.18. However, the convergence result is not valid in the case of above the upper error bound. Thus, in practical aspects, the selection of initial value and error covariance is very important to maintain the filter performance. In order to find the proper values of initial parameter, the conventional line fitting method [52, 53, 54] based on batch process is used to find the initial values by using few samples.

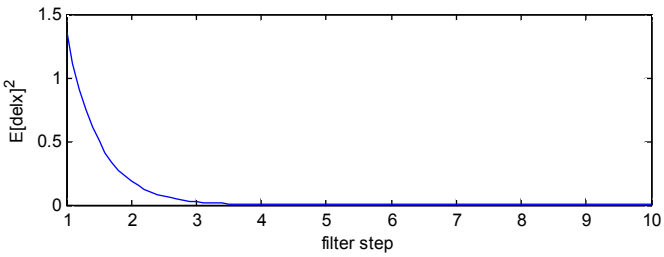

Figure 3.18 The change of the error bound

3.3.4 Modified Adaptive Fading Kalman Filter

There are many methods to adjust a Kalman gain directly or indirectly, but in this dissertation the adaptive logic is based on the R-adaptation method [55, 56, 57, 58, 59, 60, 61] for indirectly adjusting a Kalman gain, which is guaranteed to be nonnegative. In addition, the adaptive logic is designed to consider the stability of the logic and to improve the estimation performance of the measurement noise covariance.

The measurement is already modeled in eq. 3.47, but the multivariate measurement model is expressed as

$$\begin{aligned}\mathbf{y}_n &= \boldsymbol{\alpha}_0 + \mathbf{H}_n\mathbf{x}_n + \mathbf{v}_n \\ &= \boldsymbol{\alpha}_0 + \mathbf{H}_n\mathbf{x}_n + \boldsymbol{\alpha}\bar{\mathbf{v}}_n\end{aligned} \tag{3.69}$$

where $\boldsymbol{\alpha}_0$ is a $N_m \times 1$ matrix, N_m is the number of measurements and $\mathbf{H}_n$ is a $N_m \times N_s$ measurement matrix, N_s is the number of state variables. It is assumed that the noise term $\mathbf{v}_n$ is a matrix with time-varying values and modeled as $\boldsymbol{\alpha}\bar{\mathbf{v}}_n$, $\boldsymbol{\alpha}$ is a diagonal matrix with real numbers which adjusts the value of $\bar{\mathbf{v}}_n$ which is the measurement noise with a fixed covariance $\mathbf{R}_n$. The measurement residual is

$$\begin{aligned}\delta\mathbf{y}_n &= \underbrace{\boldsymbol{\alpha}_0 + \mathbf{H}_n\mathbf{x}_n + \mathbf{v}_n}_{y_n} - \underbrace{\left(\boldsymbol{\alpha}_0 + \mathbf{H}_n\hat{\mathbf{x}}_n\right)}_{y_n^-} \\ &= \mathbf{H}_n\left(\mathbf{x}_n - \hat{\mathbf{x}}_n\right) + \boldsymbol{\alpha}\bar{\mathbf{v}}_n\end{aligned} \tag{3.70}$$

The ignored error term can be considered to be measurement noise. The covariance of the simplified measurement residual is written as

$$\mathbf{C}_n^- = E\left[\delta\mathbf{y}_n\delta\mathbf{y}_n^T\right] = \mathbf{H}_n\mathbf{P}_n^-\mathbf{H}_n^T + \boldsymbol{\alpha}^2\mathbf{R}_n \tag{3.71}$$

In order to find the appropriate value of $\boldsymbol{\alpha}^2$ according to change of the measurement noise, the difference between the mean value of the variance $\hat{\mathbf{C}}_n$ and the part of $\mathbf{C}_n^-$ written in eq. 3.21 is used as

$$\boldsymbol{\alpha}^2\mathbf{R}_n = \hat{\mathbf{C}}_n - \mathbf{H}_n\mathbf{P}_n^-\mathbf{H}_n^T \tag{3.72}$$

where $\hat{\mathbf{C}}_n$ refers to the mean value of the variance, which can be calculated as

$$\hat{\mathbf{C}}_n = \begin{cases} \delta\mathbf{y}_n\delta\mathbf{y}_n^T, & n=1 \\ \dfrac{\rho\hat{\mathbf{C}}_{n-1} + \delta\mathbf{y}_n\delta\mathbf{y}_n^T}{1+\rho}, & n>1 \end{cases} \tag{3.73}$$

where ρ is weighting factor which is designed parameter.

Finally, $\boldsymbol{\alpha}^2$ can be estimated as

$$\boldsymbol{\alpha}^2 = \left(\hat{\mathbf{C}}_n - \mathbf{H}_n\mathbf{P}_n^-\mathbf{H}_n^T\right)\mathbf{R}_n^{-1} \tag{3.74}$$

However, the above equation is not guaranteed to be nonnegative. Thus, the equation should be modified by using singular value decomposition (SVD) and some definition so that $\hat{\mathbf{C}}_n - \mathbf{H}_n \mathbf{P}_n^- \mathbf{H}_n^T \geq 0$ is guaranteed. The mean value of the variance $\hat{\mathbf{C}}_n$ is assumed as a symmetric and positive definite matrix and SVD of $\hat{\mathbf{C}}_n$ is expressed as [62, 63]

$$\hat{\mathbf{C}}_n = \mathbf{D}\boldsymbol{\Lambda}\mathbf{D}^T \tag{3.75}$$

where $\boldsymbol{\Lambda}$ is a diagonal matrix with eigenvalues and $\mathbf{D}$ is an eigenvector matrix of $\hat{\mathbf{C}}_n$. $\mathbf{D}\mathbf{D}^T = \mathbf{I}$ due to the orthonormality of $\mathbf{D}$. Let $\mathbf{M}$ is defined as [55]

$$\mathbf{M} \triangleq \mathbf{D}^T \mathbf{H}_n \mathbf{P}_n^- \mathbf{H}_n^T \mathbf{D} \tag{3.76}$$

In this equation, $\mathbf{M} \geq 0$ due to $\mathbf{H}_n \mathbf{P}_n^- \mathbf{H}_n^T \geq 0$ and $\hat{\mathbf{C}}_n \geq 0$. By using the above definition, $\hat{\mathbf{C}}_n - \mathbf{H}_n \mathbf{P}_n^- \mathbf{H}_n^T$ is expressed as

$$\hat{\mathbf{C}}_n - \mathbf{H}_n \mathbf{P}_n^- \mathbf{H}_n^T = \mathbf{D}\left(\boldsymbol{\Lambda} - \mathbf{M}\right)\mathbf{D}^T \tag{3.77}$$

In order to satisfy $\hat{\mathbf{C}}_n - \mathbf{H}_n \mathbf{P}_n^- \mathbf{H}_n^T \geq 0$, an additional condition is needed. As the filter state variables are independent of each other, the diagonal terms of $\mathbf{M}$ are the only ones that remains and the other terms are set to zero. Hence, $\boldsymbol{\Lambda} - \mathbf{M}$ is a diagonal matrix and its component is set to

$$\Lambda_i - M_i = \max\left(\Lambda_i - M_i\,,\, T_i\right) \tag{3.78}$$

where $\Lambda_i - M_i$ refers to i th diagonal term of $\mathbf{\Lambda} - \mathbf{M}$ and T_i refers to i th diagonal term of $\mathbf{D}^T\mathbf{R}_n\mathbf{D}$. Thus, the α^2 is estimated as

$$\hat{\boldsymbol{\alpha}}^2 = \mathbf{D}\left(\mathbf{\Lambda} - \mathbf{M}\right)\mathbf{D}^T\mathbf{R}_n^{-1} \tag{3.79}$$

Finally, the estimated $\hat{\boldsymbol{\alpha}}^2$ is substituted in eq. 3.50 for adjusting the noise variance with the change of the measurement conditions during the filter update sequence as follows.

$$\bar{\mathbf{K}}_n = \mathbf{P}_n^- \mathbf{H}_n^T \left[\mathbf{H}_n \mathbf{P}_n^- \mathbf{H}_n^T + \hat{\boldsymbol{\alpha}}^2 \mathbf{R}_n\right]^{-1} \tag{3.80}$$

Regarding filter stability, the upper bound condition of $\hat{\boldsymbol{\alpha}}^2$ is needed to prevent instability issues which may arise when no upper bound is set [64]. The stability problem is directly related to stochastic observability, which may be violated if components of $\hat{\boldsymbol{\alpha}}^2$ ($\hat{\alpha}_i^{\,2}$) approaches infinity [46, 64]. Thus, an upper bound of $\hat{\alpha}^2$ is defined as

$$if\ \ \hat{\alpha}_i^{\,2} \geq \max\left(\hat{\alpha}_i^{\,2}\right),\ \ \hat{\alpha}_i^{\,2} = \max\left(\hat{\alpha}_i^{\,2}\right) \tag{3.81}$$

where $\hat{\alpha}_i$ refers to the i th diagonal component of $\hat{\boldsymbol{\alpha}}_i$. $\max\left(\hat{\alpha}_i^{\,2}\right)$ refers to maximum value of $\hat{\alpha}_i^{\,2}$ and its value is set to 500. In case of a single measurement model, $\hat{\alpha}^2 = \max\left(\left(\hat{C}_n - \mathbf{H}_n \mathbf{P}_n^{-} \mathbf{H}_n^T\right) R_n^{-1}\ , 1\right)$. $\mathbf{H}_n$ is a $1 \times N_s$ matrix and $\mathbf{H}_n \mathbf{P}_n^{-} \mathbf{H}_n^T$ is a scalar value.

3.3.5 Order Reduction Algorithm According to Signal Types

Regarding optimal aspects, the order of the Fourier series should be set to an optimal number that satisfies the required signal tracking performance for the different signal types. Selecting the optimal order of the Fourier series can reduce the number of state variables and reduce the computation load. If the received signal changes rapidly in the sweep period, the order of the Fourier series should be set to a high number. Otherwise, with slowly changing chirp-type sign als, the order of the Fourier series should be set to low number. Thus, in this dissertation, an optimization method, especially Powell's method [65, 66, 67, 68, 69], is used to select the optimal order of the Fourier series. Powell's method is one of the numerical optimization techniques that are classified as non-gradient methods [70, 71, 72, 73, 74], which are also called zero-order methods. Zero-order signifies derivatives are not used, but implies that function values are only used to select the search vector [74]. In general, one of the popular zero-order methods is the Powell's method which has the property of quadratic convergence and take a little more than two cycles to converge [74]. Thus, the proposed order reduction logic is based on Powell's method and conditions to derive the logic are as follows.

1) The purpose is finding an optimal value of the order from initial order N_s : $N_s > \alpha$

2) The above condition is further subject to the condition that the error of frequency tracking caused by order reduction must be less than the design threshold which is related to the minimum requirement of the frequency tracking performance. It is derived as follows: $\left|f_{N_s}(n)-f_{\alpha}(n)\right|\le T_r$

   where $f_{N_s}(n)$ is the frequency of the N_s th order Fourier series and $f_{\alpha}(n)$ is the frequency of the α th order Fourier series. T_r is the design threshold.

The error norm can be rearranged and satisfies the inequality as follows:

$$\begin{aligned}\left|f_{N_s}(n)-f_{\alpha}(n)\right| &= \left|\underbrace{f_{N_s}(n)-f_{N_s-1}(n)}_{g_{N_s}(n)}+\underbrace{f_{N_s-1}(n)-f_{N_s-2}(n)}_{g_{N_s-1}(n)}+\right. \\ &\quad \left.\cdots\underbrace{-f_{\alpha}(n)}_{g_{\alpha}(n)}\right| \\ &\le \left|g_{N_s}(n)\right|+\left|g_{N_s-1}(n)\right|+\cdots+\left|g_{\alpha}(n)\right|\end{aligned} \tag{3.82}$$

$$\le \max\left|g_{N_s}(n)\right|+\cdots+\max\left|g_{\alpha}(n)\right|\le T_r \tag{3.83}$$

where $g_i(n)=a_i\cos(iwn)+b_i\sin(iwn)$.

The maximum value of the periodic term $g_i(n)$ is expressed as $\sqrt{a_i^2+b_i^2}$. Thus, the upper bound of the error norm can be calculated as follows:

$$\left|f_{N_s}(n)-f_\alpha(n)\right|<\sqrt{a_{N_s}^2+b_{N_s}^2}+\sqrt{a_{N_s-1}^2+b_{N_s-1}^2}+\cdots\sqrt{a_\alpha^2+b_\alpha^2}$$
$$=\sum_{n=\alpha}^{N_s}\sqrt{a_n^2+b_n^2}\le T_r \tag{3.84}$$

By using the upper bound, the cost function which has no effect on the time step n can be set, for estimating α efficiently, and is defined as

$$J(x)=T_r-\sum_{n=N_s-x+1}^{N_s}\sqrt{a_n^2+b_n^2} \tag{3.85}$$

Finally, the proposed order reduction method of the Fourier series is designed to minimize the cost function and is based on Powell's method of using three points [74].

Pseudo code of the proposed algorithm is expressed as follows.

Step 1: Given an initial point x_0, interval Δx, and thresholds ε_1, ε_2,

set two points: $x_1 = x_0 + \Delta x, \quad x_2 = x_0 + 2\Delta x$

Step 2: Get $J(x_0), J(x_1), J(x_2)$

Step 3: Determine the point $x_{\min}$ in $\{x_0, x_1, x_2\}$ minimizing $J(x_i),\ i = 0,1,2$

and save $J_{\min} = \min J(x_i)$

Step 4: Get $c_1 = \dfrac{J(x_1) - J(x_0)}{x_1 - x_0}$, $c_2 = \dfrac{1}{x_2 - x_1}\left(\dfrac{J(x_2) - J(x_0)}{x_2 - x_0} - \dfrac{J(x_1) - J(x_0)}{x_1 - x_0}\right)$

Step 5: Get $x^* = \dfrac{x_1 + x_0}{2} - \dfrac{c_1}{2c_2}$, $J(x^*)$

Step 6: If $\left|J_{\min} - J(x^*)\right| \le \varepsilon_1$, and $\left|x_{\min} - x^*\right| \le \varepsilon_2$,

$\alpha = N_s - round(x^*) + 1$; Stop,

else ; Continue

Step 7: Reassign: $x_2 \leftarrow x^*$, $x_1 \leftarrow x_{\min}$,

x_0 is set in $\{x_0, x_1, x_2\}$ except $x_{\min}$, Go to Step 4

where $round(\ )$ is a function which rounds the elements to the nearest integers. In this code, $x_0 = 1,\ \Delta x = 2,\ \varepsilon_1 = \varepsilon_2 = 0.01,\ T_r = 0.005.$ The range of x is limited to $x \in [1,\ N_s)$. N_s is the maximum order of the Fourier series and it is set to 5 because of computational complexity. The computational complexity of the proposed algorithm is $O\left((2x+1)^3\right)$, and x refers to the order of the Fourier series. The selected maximum order of the Fourier series is enough to track the chirp frequency whose sweep rate is $1 \sim 2\times10^{12}\,Hz/\sec$ [18, 43] under the required frequency tracking error for mitigating the interference signal [28]. However, if higher order (above five) is selected, the computational complexity dramatically increases by $O\left((2\Delta x+1)^3\right)$ [46]. Where Δx is an order increment compared with five. Finally, α obtained in step 6 is set to an optimal order of the Fourier series according to the type of the frequency.

3.3.6 Simulations and Analysis

In the simulations, frequency tracking performance of the proposed algorithm is evaluated and compared with that of conventional algorithms and the proposed order-reduction algorithm based on the optimization algorithm is also verified for three types of chirp interference. The conventional methods were selected to be: an adaptive fading Kalman filter without period estimation (AKF) [35] an adaptive fading Kalman filter with period estimation (PAKF) [28]; and, a hybrid EKF based on the Fourier series without the order-reduction logic (HEKF). Filter models of the AKF are the same as that of the proposed algorithm. For the AKF, a Kalman gain is increased by α_n, which refers to $\mathbf{K}_n = \alpha_n \mathbf{P}_n^- \mathbf{H}^T \left[\mathbf{H}\mathbf{P}_n^- \mathbf{H}^T + \mathbf{R}_n \right]^{-1}$. The increase of the Kalman gain is to depend more on measurement information and consequently to increase the sensitivity of the response to frequency change. Thus, but for the lack of a sweep period estimation method the filter can track a chirp-type interference. In simulations, only the chirp-type interference is received and the signal power of the received GNSS signal is -130dBm, the overall noise floor is at -114dB/MHz and the J/S is set to 30dB.

Frequency tracking results of simulations for the three types of chirp interference are shown in figures 3.19, 3.20, and 3.21 for AKF, PAKF and the proposed algorithm. Figure 3.19 “true” data refers to a linear chirp-type interference which is made by the a fifth-order Fourier series, figure. 3.20 “true” data refers to a linear chirp-type interference without a dramatic change, which is modeled by a second order Fourier series, and figure 3.21 “true” data is a nonlinear chirp-type interference made by a fourth-order Fourier series.

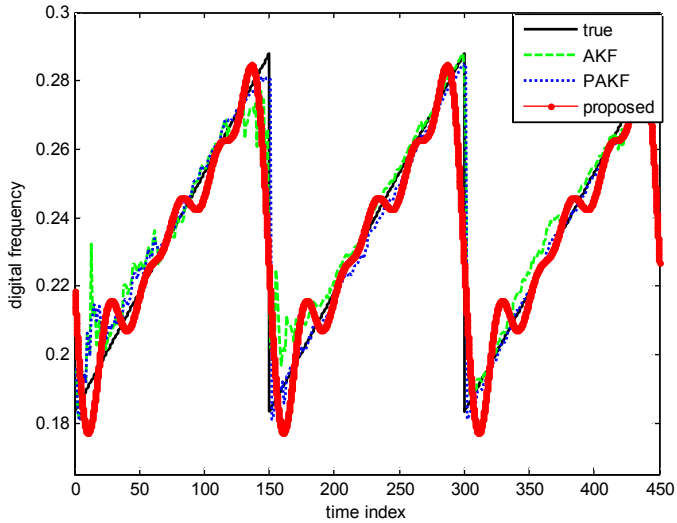

Figure 3.19 Type 1 chirp interference with dramatic change

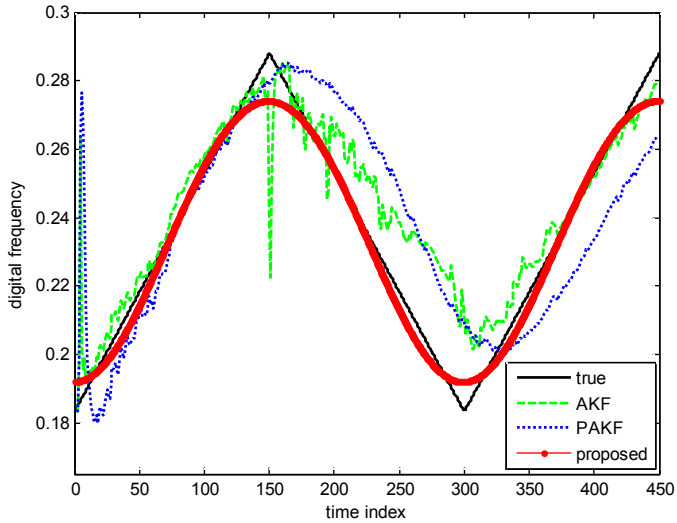

Figure 3.20 Type 2 chirp interference without dramatic change

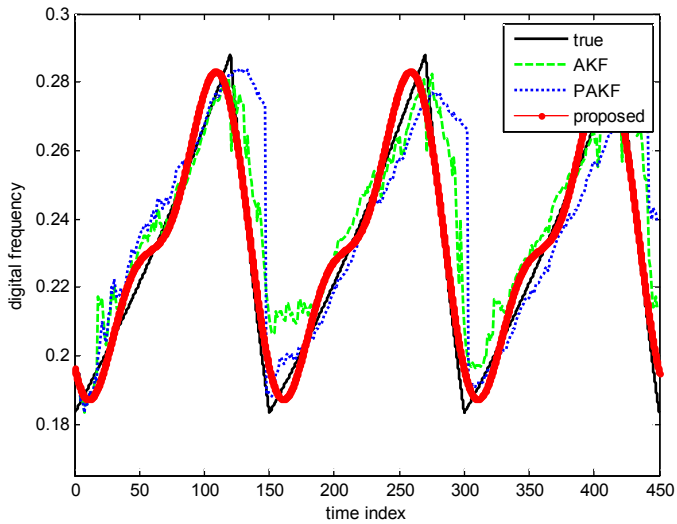

Figure 3.21 Type 3 chirp interference with nonlinear change

With AKF, the convergence rate of the filter is improved by increasing the Kalman gain and prior predicted error covariance, so frequency tracking is possible. However, increasing the Kalman gain also leads to an estimation error caused by depending too much on the measurement in the beginning of the seep period (figure 3.19). The AKF has a severe tracking error when the simulation time index exceeds the first period, after a time index of ~150 as shown in figure 3.20, because the convergence speed of the filter is slower than the change rate of frequency near the peak of the frequency. In figure 3.21, the AKF does not track the nonlinear chirp-type interference due to the linear state model of the filter. With PAKF, it has the best performance of all the methods when the linear chirp-type interference is received as shown in figure 3.19 because of the sweep period estimation logic in the frequency-tracking algorithm. However, the sweep period estimation logic only works well on linear chirp-type interference. If another type of chirp interference is received, the sweep period estimation logic cannot estimate the period. For that reason, filter state and error covariance is not reinitialized at the appropriate time. This problem causes the severe tracking error shown in figures 3.20 and 3.21.

Comparing the results for the frequency estimation, the proposed algorithm does not have better tracking performance than AKF and PAKF with linear chirp-type interference shown in figure 3.19, but it maintains tracking performance regardless of the signal type. For chirp-type interference without dramatic changes (figure 3.20) and for nonlinear chirp-type interference (figure 3.21), the proposed algorithm has better performance

compared to that of PAKF due to the nonlinear filter state model designed using a Fourier series. The frequency estimation RMSE of each filtering method is written in Table 3.1 for Monte Carlo simulations which are 500 independent runs of the frequency tracking simulations for three types of chirp interference.

Table 3.1 RMSE of frequency tracking algorithms

	Type 1	Type 2	Type 3
AKF	0.0090	0.0310	0.0137
PAKF	0.0042	0.0363	0.0207
Proposed	0.0091	0.0042	0.0061

In figure 3.22, 3.23, and 3.24, the performance of the order-reduction logic is shown according to interference types. The initial order of the Fourier series is set to 5 in this simulation and it is confirmed that the proposed order-reduction algorithm can adjust the order of the Fourier series according to the received signal types. If the received signal changes rapidly in the sweep period, the order of the Fourier series is set to 5. Otherwise, for slowly changing chirp-type signals and for nonlinear chirp-type interferences, the order of the Fourier series is set to 2 and 4, respectively. In these figure, there are transition period which is less 5 time index because of filter's tracking convergence rate, but few time index later, the estimate order converges to true value.

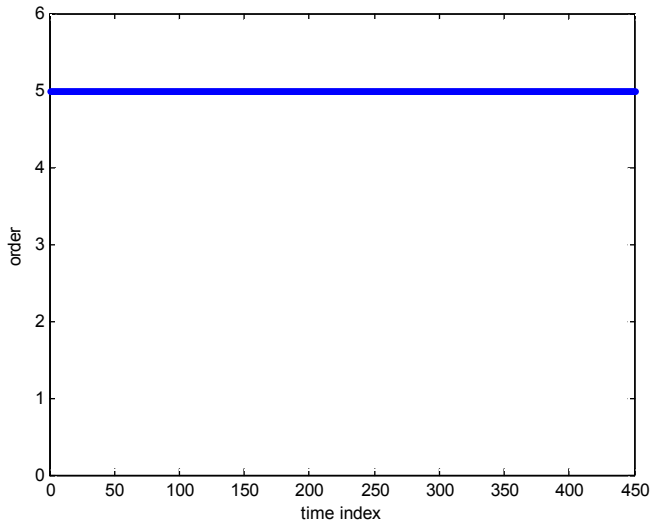

Figure 3.22 The estimate of the order of Type 1 chirp interference

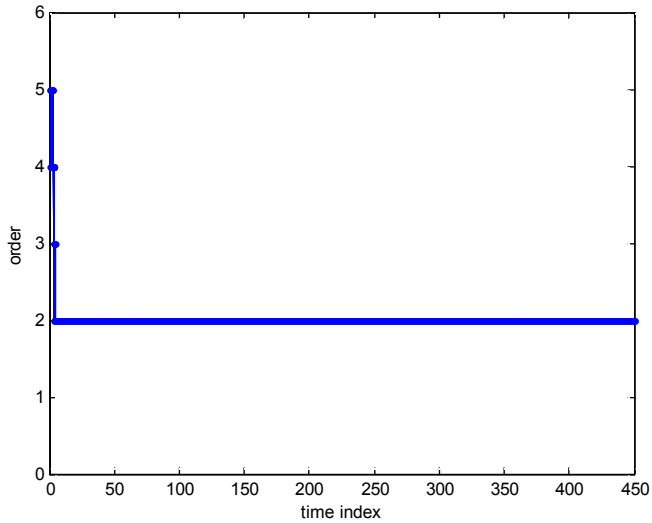

Figure 3.23 The estimate of the order of Type 2 chirp interference

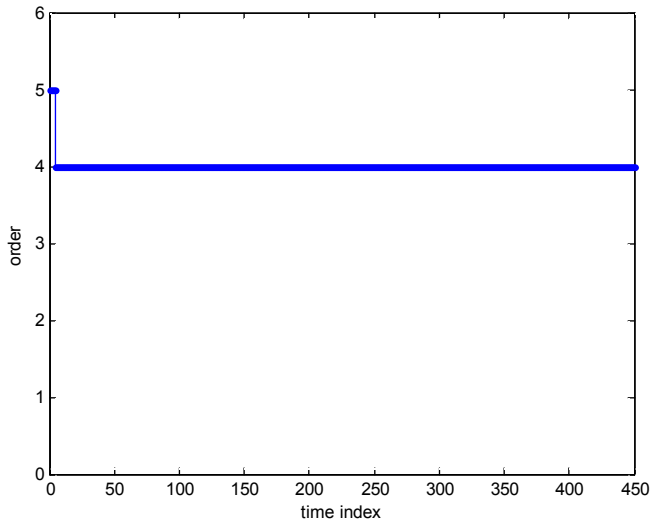

Figure 3.24 The estimate of the order of Type 3 chirp interference

In the last simulation, the performance of the adaptive logic is verified compared to that of the HEKF based on the Fourier series with/without adaptive logic when the linear chirp-type interference is received with the measurement error.

In figure 3.25, the HEKF with adaptive logic (proposed algorithm) has better performance than the HEKF without the adaptive logic. The RMSE of the proposed algorithm is 0.0111 and that of the HEKF is 0.0124. The calculation error of measurement when $r(n)=0$ expressed in the section 3.2.1 has a large effect on frequency tracking performance periodically. However, the modified adaptive logic can reduce the error effect as shown in figure 3.25.

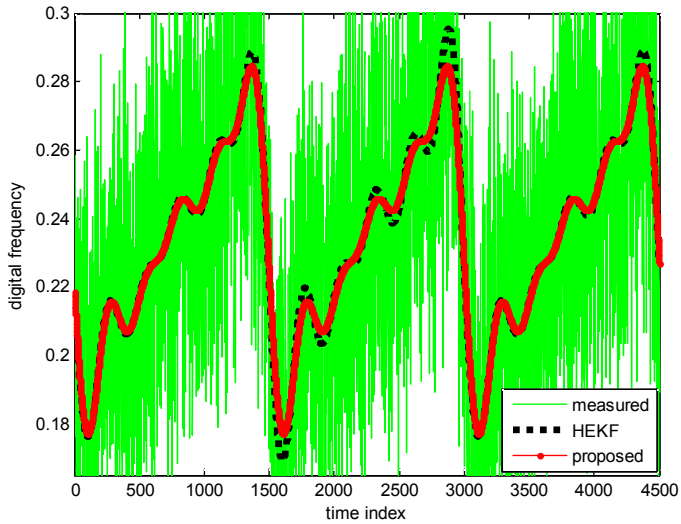

Figure 3.25 The adaptive logic performance

In this chapter, an interference tracking algorithm is proposed that utilizes an adaptive hybrid EKF that is based on the Fourier series and also an order-reduction algorithm based on Powell's method to estimate the frequency of various chirp-type interferences. The proposed adaptive logic always guarantees the nonnegative aspect of the fading factor and reduces the measurement error effectively. In addition, the optimal order of the Fourier series for the signal type is selected by the proposed order-reduction algorithm. Simulation results show that, compared to conventional methods, the proposed algorithm can more efficiently track various types of chirp interference.

Chapter 4. Interference Detection and Mitigation

For effective GPS interference mitigation, interference detection metrics should be defined in order to monitor an unexpected behavior of the GNSS receiver. Detection parameters are statistically characterized in order to describe the behavior in nominal operative conditions and in presence of interference. They can be defined by Monte-Carlo simulation or test campaigns. Based on the statistical behavior of the parameter, threshold can be defined on a desired level of false alarm probability. Then, if the anomaly is detected, countermeasures can be implemented from simple warning to full mitigation.

There are various methods to detect GNSS interference. They are mainly classified as the pre-correlation detection method and the post-correlation detection method depending on where the algorithms are applied as shown in figure 4.1. Antenna, AGC and ADC have been used to detect and characterize interference in pre-correlation techniques [75-78], while receiver observables like C/No, phase distortion, and pseudo-range step measurements are used for post-correlation techniques [79-82]. For most civil applications, post correlation detection methods using receiver observables have been preferred because it does not require additional hardware modification. However, post-correlation methods can be used only when a receiver is tracking GNSS signal, so the methods are not adequate for characterization of intentional interference whose power is above a civil receiver's tracking threshold. In

addition, post-correlation methods require more time to detect interference than pre-correlation methods because C/No estimation requires an averaging time of approximately 1 second to achieve unbiased estimation results [82]. Thus, in this dissertation, pre-correlation detection method is selected to detect the GPS interference.

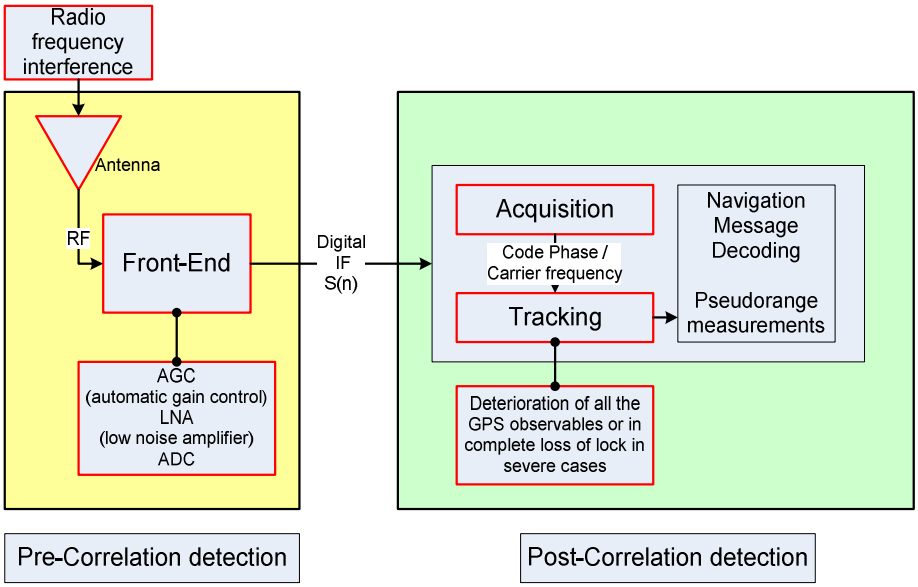

Figure 4.1 Types of interference detection and mitigation methods

4.1 Pre-Correlation Detection Method

An interference detection method is proposed that uses the adaptive IIR notch filter parameters: $r_0(n), r_1(n)$, to estimate the center frequency of the interference signal, and to derive $\cos(\omega_i)$. The characteristic of AGC gain is also used to detect the interference. In this section, the characteristics of detection parameters and AGC gain are presented when the interference is received.

4.1.1 Characteristics of Detection Parameters

The parameters have unique characteristics, according to the type of incoming interference signal [10]. The analysis of the parameter characteristics is performed when J/S of the interference is above 30dB, which severely affect the navigation accuracy of the GNSS receiver [3]. When the received CWI's J/S is above 30dB, $r_0(n)$ tends to converge to a certain value. If the interference signal power increases, the magnitude of $r_0(n)$ also increases, because it is the energy of the AR block output signal. figure 4.2 shows the $r_0(n)$ characteristic with, and without, interference signals. When the input signal is a swept CWI, that has a linearly increasing interference center frequency, the value of $r_1(n)$ linearly decreases. This result is shown in figure 4.3. From the characteristics of $r_0(n)$ and $r_1(n)$, it is possible to detect interference signals, such as single-tone, swept CWI (chirp-type interference)and band-limited white Gaussian noise (BLWN) by selecting appropriate thresholds.

A noise process which has non-zero constant power spectrum density (PSD) over a finite frequency band is called BLWN and it is modeled by

$$I_{BLWN}(\omega) = \begin{cases} \frac{N_0}{2} & |\omega - \omega_0| < \frac{B}{2} \\ 0 & otherwise \end{cases} \tag{4.1}$$

where $I_{BLWN}(\omega)$ is the PSD of the BLWN, N_0 is called the intensity of the white noise and $\omega_0 = 2\pi f_{IF}$. B is the bandwidth set to 4MHz.

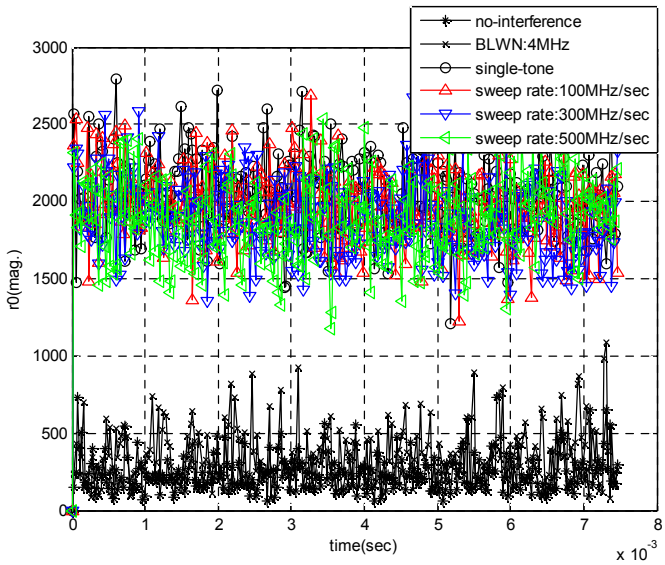

Figure 4.2 $r_0(n)$ value with/without interference signal (J/S is 30dB)

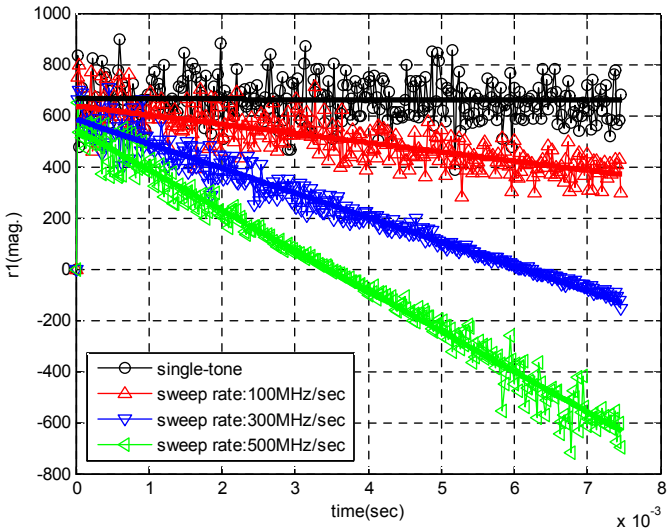

Figure 4.3 $r_1(n)$ value for swept continuous wave interference with varying sweep rate (J/S is 30dB)

However, these parameters depend on two conditions: input signal power and frequency of the input signal, so that it is difficult to decide the threshold which is used to recognize the existence of GPS interference. Thus, in this dissertation, AGC gain is used to detect the GPS interference which depends on only input signal's power. In addition, by using AGC gain, the notch depth of the second order IIR notch filter is adjusted. The detail explanation is written in the next section.

4.1.2 Characteristics of AGC Gain

The automatic gain control (AGC) in a GNSS receiver is used to adjust the power level of the intermediate frequency (IF) signals at the input to the analog-to-digital converter (ADC), to minimize the quantization loss [13]. It has been investigated before as an interference assessment tool [3,40]. Interference is a main source that changes the AGC gain, because the power of the GNSS signal is below the thermal noise floor. Therefore, AGC can be a valuable tool for detecting interference [41, 75]. In this dissertation, the value of AGC gain is examined according to the increasing power of interference, and the results are used for detecting the existence of interference sources. When interference is received, the action of the AGC is to reduce the gain, in order to maintain constant power level at the input of the ADC.

The GNSS signal and interference simulator adapted an exponential AGC model, which is controlled by a digital feedback loop and 8 bit ADC. The AGC gain, G_{AGC} is modeled as

$$G_{AGC} = \alpha e^{\beta V_C} \tag{4.2}$$

where V_C is the AGC control voltage, α is an AGC gain coefficient, and β is an AGC control voltage coefficient [41].

The action of AGC is shown in figure 4.4, which shows that the AGC gain is reduced when interference is received whose J/S is 30dB.

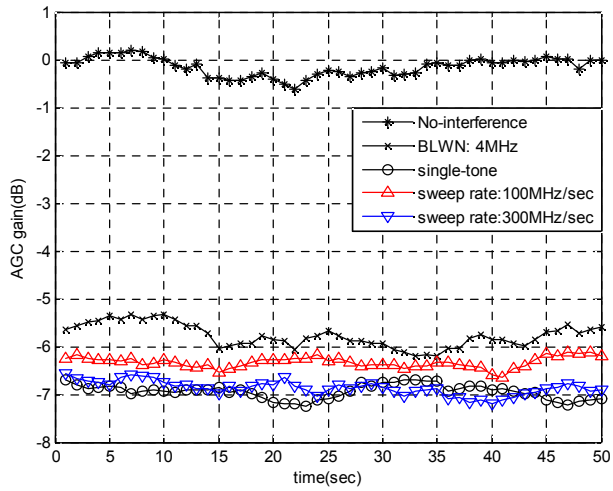

Figure 4.4 The characteristic of AGC gain (J/S is 30dB)

The selection of detection threshold has a great effect on the performance of the interference detection. The mean of G_{AGC} is compared to a threshold for the interference signal detection. If the mean of G_{AGC} is above T_G , the detection method classifies the received signal as no interference signal. T_G is selected to detect an interference signal whose J/S is more than 30dB, which seriously affects the accuracy of the GPS [3]. Selection of thresholds is as follows.

T_G is determined by

$$T_G = \frac{\mathbf{AGC}_{gain\_30} + \mathbf{AGC}_{gain\_ni}}{2} \tag{4.3}$$

where $\mathbf{AGC}_{gain\_30}$ is the mean value of G_{AGC} when the interference whose J/S is 30dB is received, $\mathbf{AGC}_{gain\_ni}$ refers to the mean value of G_{AGC} without interference.

To evaluate the performance of interference detection, the detection probability has been calculated by Monte Carlo simulations, which are on the basis of 3000 independent runs of the proposed detection method every 5dB of J/S, when the interference exists in the received signal.

The detection probability is defined as

$$P_{\det} = \frac{\mathrm{N}_{if}}{\mathrm{N}_{s}} \tag{4.4}$$

where the numerator refers to the number of correct interference detections and the denominator refers to the number of iterations. Figure 4.5 refers to the detection probability of GPS interference and it is shown that the detection method using AGC gain can detect the interference perfectly, whose J/S is above 30 dB.

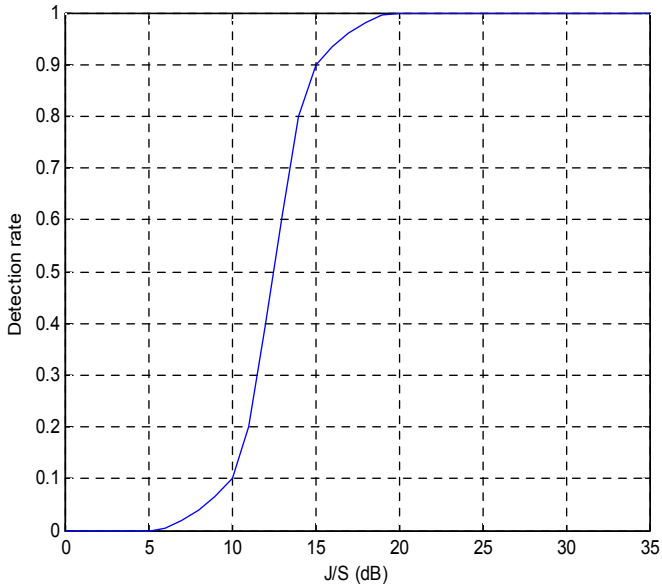

Figure 4.5 Detection probability of the interference signals

4.2 Notch Filter Based Interference Mitigation Method

Various GNSS interference mitigation methods have been proposed in earlier papers, and most are based on signal cancelation, which is a popular topic in relation to signal processing [83, 84]. The one of the interference mitigation methods involves the use of a digital notch filter, which is known as a particularly effective method for eliminating continuous wave interference.

The IIR notch filter requires a much shorter filter length than the FIR filters, and it can remove interference signals or narrow-band noise effectively [26]. In addition, it has been shown that the lattice IIR notch filter provides better convergence properties and more accurate frequency estimates compared to direct form implementations [8]. In this dissertation, a lattice IIR notch filter is used for the mitigation method, and the frequency tracking result is used to set the notch center frequency.

The notch filter is able to place a deep null in correspondence with the frequency of the interference, and, if the frequency is properly updated from the frequency tracking results, to track interference frequency variations. In order to remove the interference accurately and acquire the GNSS data in the mitigated signal from the notch filter, the frequency estimation error should be small. Thus, the requirement of the mitigation algorithm using the notch filter is determined through the Monte Carlo simulations shown in figure 4.6, in which the probability of GNSS acquisition is calculated according to the frequency tracking error. In addition, it is assumed that two types of

interference (single-tone and chirp-type interference) present respectively with GPS data in this simulation. The acquisition probability is defined as

$$P_a = \frac{N_a}{N_s} \tag{4.5}$$

where the numerator refers to the number of successful instances of GPS signal acquisition using the mitigation data obtained from the notch filter with the tracking error. The type of error is assumed to be additive white Gaussian noise. The denominator refers to the number of simulations. As shown in figure 4.6, if the frequency tracking error is less than 300 KHz, it is possible to acquire the GPS signal using the mitigation data.

In addition, it is necessary to adjust the depth of the notch in order to reduce GPS data distortion while removing the interference effectively. By the notch filtering with infinite depth at the GPS signal frequency, the GPS information as well as the interference is removed. Therefore, the adjust parameter of notch depth is added to the general notch filter and expressed as [8]

$$\bar{H}(z) = \frac{1 - \cos\omega_i (1 + r_2) z^{-1} + r_2 z^{-2}}{1 - 2(1 + r_1 r_2)\cos\omega_i z^{-1} + r_1 r_2 z^{-2}} \tag{4.6}$$

where r_2 control the depth and r_1 (it is r in eq. 3.1) adjust the width of notch. Appropriate r_1 is selected based on frequency tracking error bound, which is set to [85, 86]

$$r_1 = \frac{1-\tan(BW/2)}{1+\tan(BW/2)} \tag{4.7}$$

where BW is the -3dB bandwidth of the notch and is set to 0.988 in order to include the all frequency bandwidth of estimated frequency in the notch. If r_1 is set to 0.988, bandwidth, BW is 0.012 (if sampling frequency is 38.192MHz, bandwidth is near to 460kHz).

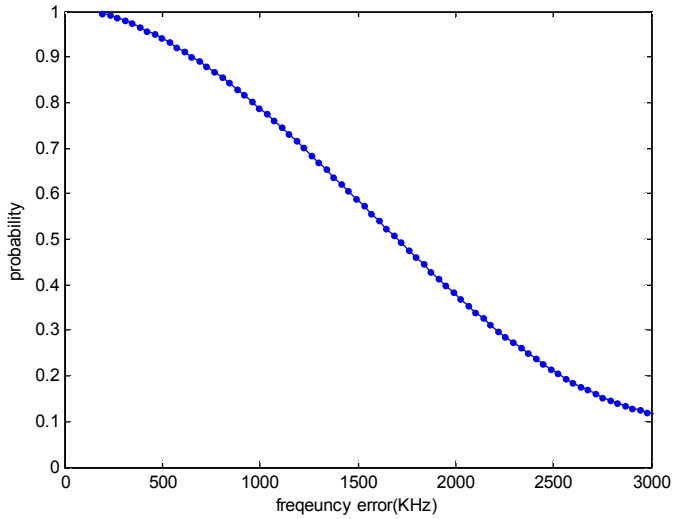

Figure 4.6 The requirement of the mitigation algorithm [28]

However, in the case of the notch depth, the adaptive logic is needed to adjust the depth according to the power of incoming interference. The adaptive logic of adjusting the notch depth is based on the inequality relationship between input signal's power and output signal's power and expressed as [8]

$$P_{jo} + \sigma_{wo}^2 \le \sigma_{wi}^2 \tag{4.8}$$

where P_{jo} refers to output power of the interference, σ_{wo}^2 is variance of noise passing through the notch filter, and σ_{wi}^2 is variance of input signal's noise. The inequality equation means that the notch depth is adjusted as the output signal's power is similar to that of input signal's noise variance. According to [8], these values are expressed by the notch filter parameters r_1 and r_2 .

$$\frac{A^2}{2}\frac{\left(1-r_2\right)^2}{\left(1-r_1 r_2\right)^2} + \sigma_{wi}^2 \frac{1+\left(1-2r_1\right)r_2^2}{1-r_1^2 r_2^2} \le \sigma_{wi}^2 \tag{4.9}$$

If the above inequality is divided by σ_{wo}^2 and rearranged as

$$\frac{A^2}{2\sigma_{wi}^2}\frac{\left(1-r_2\right)^2}{\left(1-r_1 r_2\right)^2} + \frac{1+\left(1-2r_1\right)r_2^2}{1-r_1^2 r_2^2} - 1 \le 0 \tag{4.10}$$

where the effect of output interference power indicated by the first term decrease as the r_2 increases. However, the second term in eq. 4.9 can be considered as the self-noise term, which shows larger value as the increases (the notch depth becomes deeper). Hence, the optimal r_2 can be found by minimizing the cost function which minimizes the above inequality equation.

The cost function is defined as

$$C(r_2) = \frac{A^2}{2\sigma_{wi}^2} \frac{(1-r_2)^2}{(1-r_1 r_2)^2} + \frac{1+(1-2r_1)r_2^2}{1-r_1^2 r_2^2} \tag{4.11}$$

In order to find the optimal r_2, $C(r_2)$ is differentiated as

$$\begin{aligned} \frac{\partial C(r_2)}{\partial r_2} = & \frac{A^2}{2\sigma_{wi}^2} r_1^2 r_2^3 + \left(2r_1 \frac{A^2}{2\sigma_{wi}^2} - r_1^2 \frac{A^2}{2\sigma_{wi}^2} + r_1^2 - r \right) r_2^2 \\ & + \left(1 - r_1 +_1 \frac{A^2}{2\sigma_{wi}^2} - 2r_1 \frac{A^2}{2\sigma_{wi}^2} \right) r_2 - \frac{A^2}{2\sigma_{wi}^2} = 0 \end{aligned} \tag{4.12}$$

The roots are expressed as a function of $A^2 / 2\sigma_{wi}^2$ which denotes the jammer to noise ratio (JNR) and notch filter parameters. Finally, one of the roots is selected in the range $[0, 1]$ and this value is used to set r_2 which adjust the notch depth as shown in figure 4.7. The variation of optimal r_2 with respect to Jammer to signal ratio is shown in figure 4.8. Power of input signal can be estimated by AGC gain in the front-end of the receiver. However, in this dissertation, analysis results on the relation between the received signal

power and AGC in [13] is adopted and we only have focused on the system modeling in terms of theoretical analysis in order to derive the proposed algorithm simply. The next section shows that the performance of the proposed algorithm satisfies the mitigation condition and that it can remove interference.

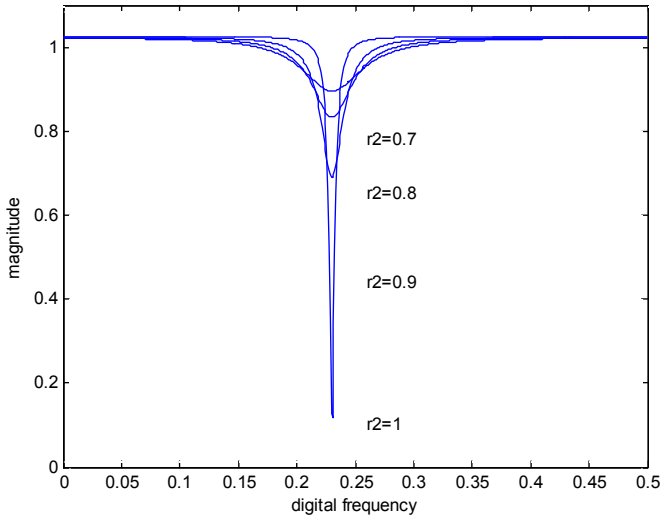

Figure 4.7 The change of notch depth according to r_2

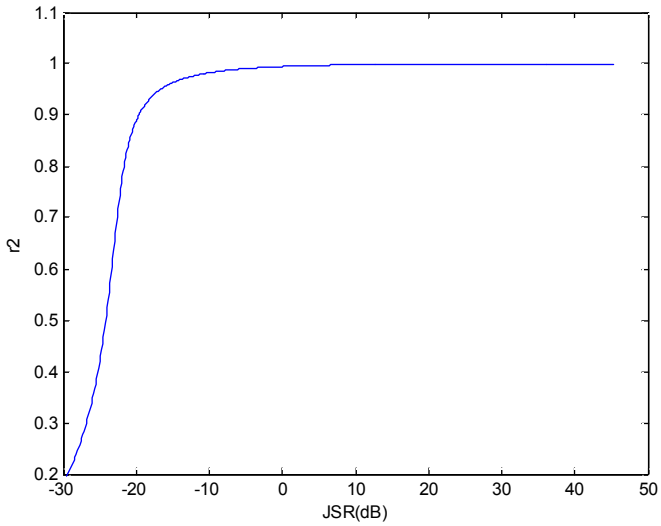

Figure 4.8 The change of r_2 according to JSR

4.3 Performance Analysis by Using a Software-Defined Radio

In simulations, the mitigation performance is verified by using a software-defined radio (SDR) [87] to detect the presence of the GPS navigation data as the mitigated signal passes through the notch filter. A software GPS receiver is utilized to develop an interference assessment model [87, 88]. However, various interference signal data are required for the interference assessment. Therefore, the GPS interference signal simulator is designed to generate IF signal data which can be directly used for the software GPS receiver. The interference simulator can generate user specified interferences repeatedly, so it can be used for interference signal characterization and detection algorithm research. The simulator gets signal parameters from a user and generates GPS L1 signal, noise and interference signals. The generated signals are processed by band pass filter, AGC, and ADC module and saved in a binary file. Figure 4.9 shows the concept of the GPS interference simulator [3]. The simulator can generate various types of GPS interference. The simulated signal data were verified by theoretical evaluation of signal spectrum and used for interference effect assessment and interference detection and mitigation algorithm research as reference signal data [3]. In simulations, two process of GPS receiver are used to verify the existence of navigation data in the mitigated signal: acquisition, tracking.

Settings of acquisition and specification of tracking loop in the SDR are summarized in Table 4.1. The average signal power of the received GPS

signal is -130dBm, the overall noise floor is set to -114dB/MHz, and the J/S is 30dB.

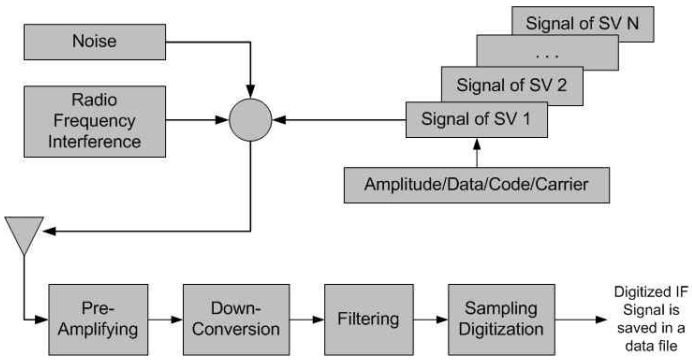

Figure 4.9 Concept of GPS interference simulator [3]

Table 4.1 Settings of the GPS SDR [87]

Acquisition		
Accumulation time	5ms (Non-coherent method)	
Fine tuning	10ms data used (Doppler frequency resolution)	
Tracking loop		
Carrier tracking	Noise bandwidth	25 Hz
	Loop filter	The second order PLL
	Discriminator	$Tan^{-1}(Q/I)$
Code tracking	Noise bandwidth	2 Hz
	Loop filter	DLL with 6 correlators
	Discriminator	$\{(I_E^2+Q_E^2)-(I_L^2+Q_L^2)\} / \{(I_E^2+Q_E^2)-(I_L^2+Q_L^2)\}$
	Code space	0.5 chip

In the case of GPS signal, the received signal includes the single channel of the GPS signal whose PRN number is 3.

Figures 4.10 and 4.11 illustrate the results of the mitigation in time-frequency domain. In figure 4.10, sub figures show the time evolution of the frequency content of the received data. In this figure, red color refers to high value of power sepctruem and blue color denotes low value of power spectruem. The frequency component of the chirp-type interference is dominant in the received signal, as shown in the figures, and there are three types of chirp-type interference in each sub figures. Sweep rate of all types is set to 1×10^{12} Hz/s, minimum frequency is set to 7MHz, maximum frequency is 11MHz, and sampling rate is 38.192MHz. Figure 4.11 shows the time evolution of the frequency content in the mitigated signal using the notch filter. In these figures, the notch filter which uses the frequency tracking results clearly removes the chirp-type interference.

Figures 4.12 and 4.13 indicate the detection of a one-channel GPS L1 C/A signal (PRN 3). When a mitigation method is not used, the cross-ambiguity function [87]is corrupted by interfering components that mask the presence of the useful GNSS signal, as clearly shown in figure 4.12. As the interference components are removed by the mitigation algorithm, the cross-ambiguity function has one peak, as shown in figure 4.13. Thus, the code phase and Doppler frequency of the GNSS satellite's one channel are obtained using the mitigated signal, and these results are identical to those of the original GNSS signal.

The estimation error of code phase and Doppler frequency is about 0.3 chip and 53 Hz (after fine tuning [87]), respectively. These results show that GPS signal tracking is possible by using the mitigated signal.

Figure 4.14 and 15 show GPS tracking result, respectively compared with a normal condition of PRN 3. In figure 4.14, variation of feedback values to numerically controlled oscillator (NCO) in the case of the mitigated signal is bigger than that of a normal condition signal because the signal power is reduced after passing through the notch filter. If the signal quality decrease (signal power reduction), the tracking loop does not works well compared to normal condition. For that reason, the feedback values does not converge to certain values, but change significantly. If tracking performance of code phase decrease, the feedback value of DLL has jitters, which cause the pseudorange error as shown in figure 4.15.

In this section, it is confirmed that the mitigation method based on the notch filter can reduce the effect of chirp-type interference without the distortion of the GPS signal. However, in order to apply a practical mitigation system, the process time of the proposed algorithm should be reduced. The relative process time of all algorithms which is proposed in the dissertation is obtained by MATLAB function (tic/toc) and is shown in Table 4.2. The time in the table is not real computational time but the processing time which is obtained by MATLAB function (it includes processing time of background software). In addition, the processing time depends on specifications of computer and process environment of software. The proposed algorithm is classified as three parts; frequency calculation, frequency estimation, and

mitigation. In the table, the mitigation part takes too much portion of process time because a cubic equation, eq. 4.12 is solved in the process for adjusting the notch depth of the notch filter. The total process time is 4.1×10^{-3} sec and is longger than a sampling period, 2.5×10^{-8} sec. Thus, algorithm optimization for reducing process time and high performance computer are needed to apply the proposed algorithm to the mitigation system based on sequential method.

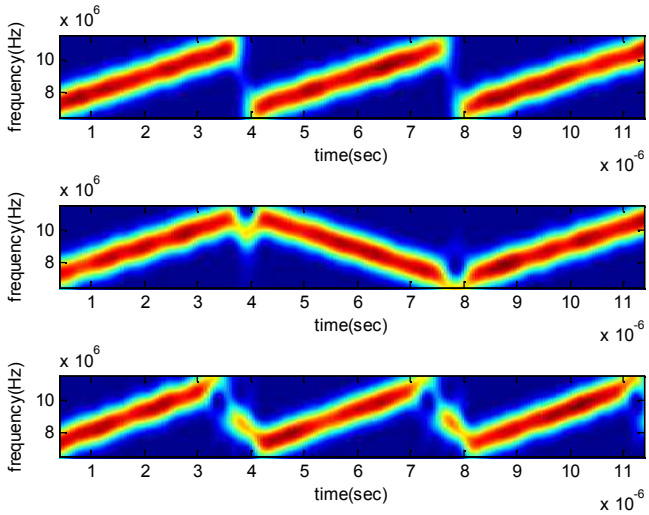

Figure 4.10 Time-frequency evolution of received signal

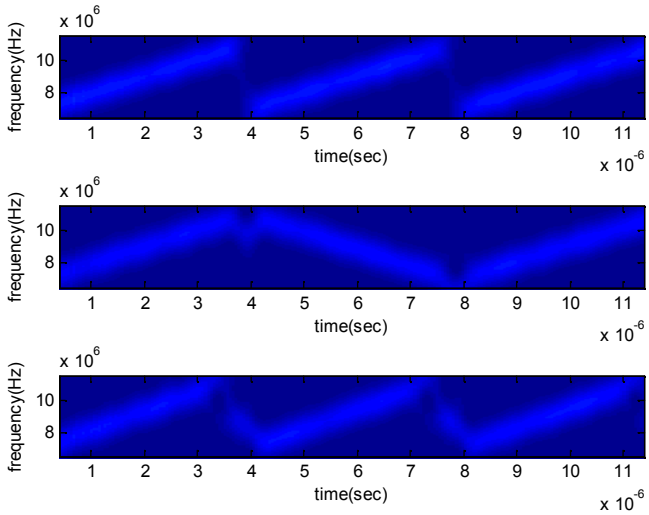

Figure 4.11 Time-frequency evolution of mitigated signal

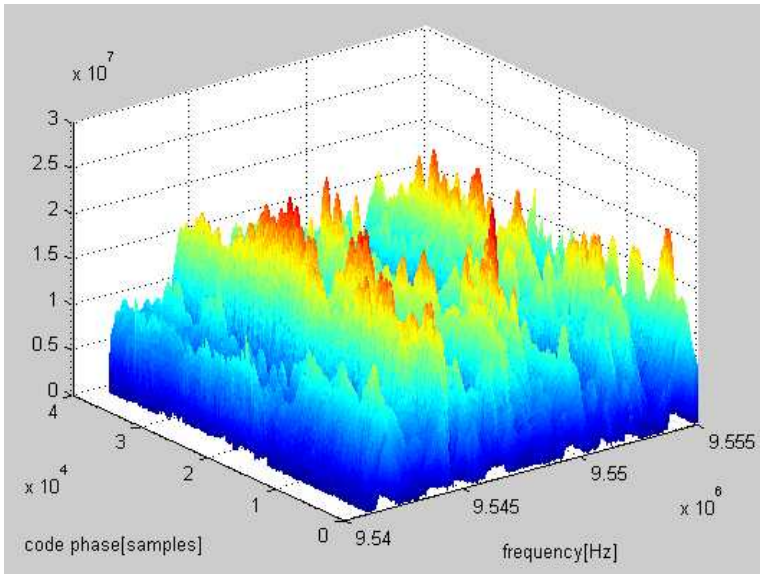

Figure 4.12 The cross ambiguity function of the received signal

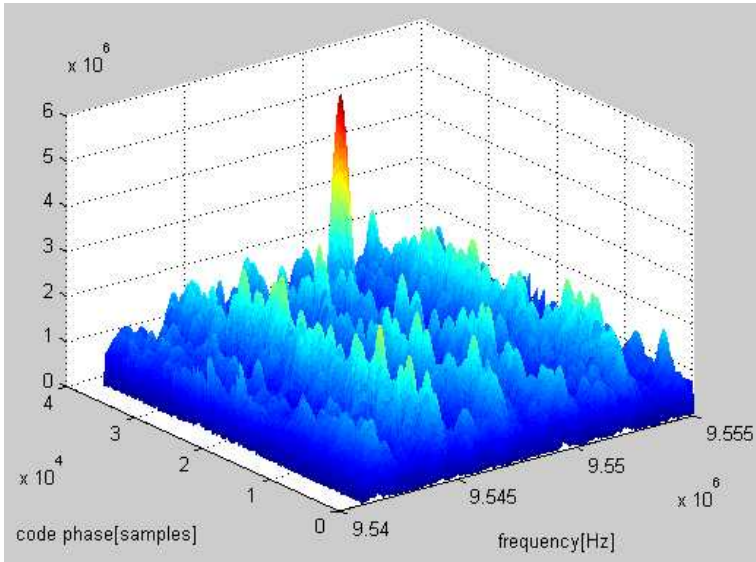

Figure 4.13 The cross ambiguity function of the mitigated signal

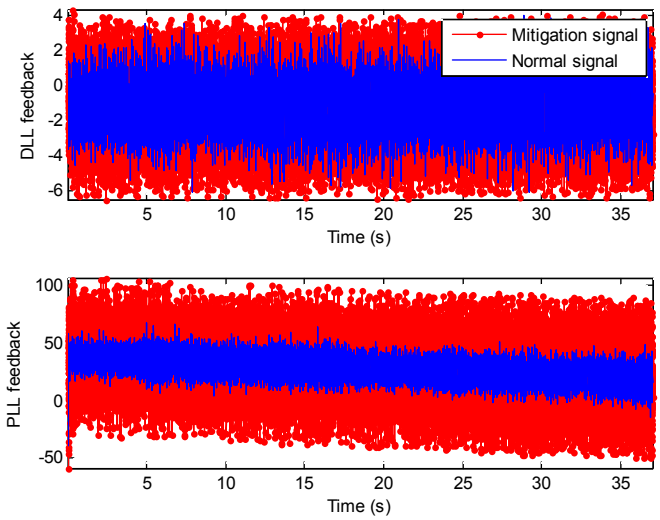

Figure 4.14 The feedback values from tracking loop to NCO

(top: DLL, bottom: PLL)

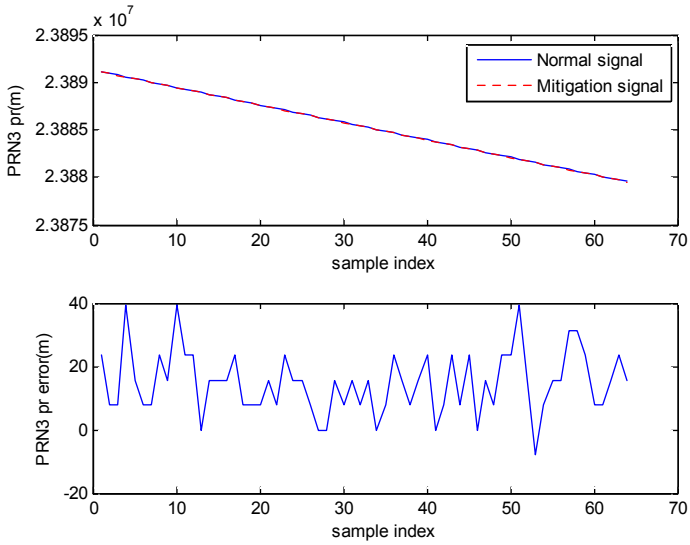

Figure 4.15 The comparison results of the pseudorange

(top: pseudorange, bottom: pseudorange error)

Table 4.2 Processing time of the proposed algorithm

State	Process time (msec)	Computational rate (%)
1 Frequency calculation	0.014	0.34
2 Frequency estimation	0.159	3.87
3 Mitigation	3.913	95.43

Chapter 5. Conclusions

GNSS are space-based satellite navigation systems that provide autonomous geo-spatial positioning with global coverage. In order to send the information of satellites to GNSS receivers on the ground, the navigation system uses a radio frequency (RF) signal. However, its received signal power is relatively weak, because of the long distance between satellites and GNSS receivers. For this reason, it is easy for other RF signal sources to degrade the performance of GNSS receivers, by making acquisition and tracking of the satellite signals difficult or impossible. In particular, an intentional RF signal that degrades the navigation accuracy or causes a complete loss of receiver tracking is called a GNSS interference or jamming signal. Such interference is a major threat to civil aviation using GNSS. In order to deal with this threat, detecting and tracking interference are important for safe GPS operations.

Previous works have focused on detecting the existence of GPS interference using an adaptive notch filter. These approaches are limited when used to detect and track chirp-type interference because the fast sweep rate of this type of interference degrades the signal tracking performance of an adaptive notch filter. In addition, these methods also have limitations when the quality of the measurement suddenly deteriorates. In these cases, the tracking and mitigation performance of the adaptive notch filter is degraded on account of the simple filter structure, which does not include a robust algorithm. Thus, it is necessary to use a model-based tracking algorithm for

chirp-type interference or other GPS interference types when the measurement noise increases.

In this dissertation, two Kalman filter based interference frequency tracking algorithms are proposed and the notch filter based mitigation algorithm is applied to reduce the effect of the interference by using frequency tracking results.

First of all, a novel interference identification and tracking algorithm which uses an adaptive fading Kalman filter, a pattern recognition algorithm with LPD, and a pattern enhancement algorithm based on the AR model is proposed. It consists of four parts: the interference frequency calculation, interference identification, frequency tracking, and mitigation. In the first step, the instantaneous frequency is calculated using the three samples of the received signal mentioned in the previous section. In the second step, the LPD creates the peak pattern to estimate the sweep period of the chirp-type interference and to generate the pulsed signal used for the classification of the interference. The pattern enhancement algorithm is also used to improve the peak detection performance, and the value of the enhanced peak pattern is utilized to generate the pulsed signal so that the type of interference can be labeled in the interference classification logic. In the third step, the frequency tracking logic estimates the interference frequency using the interference identification result and the estimated time index of the sweep period from the previous step. Comparing the frequency estimation results of simulations, the proposed algorithm demonstrates better tracking performance than the DKF and conventional AKF methods, as the proposed algorithm resets the filter at

the beginning of the sweep period by means of period estimation. The frequency estimation RMSE of the proposed algorithm is 0.0071, that of the DKF method is 0.0220, and that with the AKF is 0.0115 in the case of linear chirp-type interference.

However, due to the limited performance of LPD which is used to estimate the sweep period of the interference, the algorithm can only track linear chirp-type interference which has a dramatic change at the end of sweep period. If another chirp-type which does not have the dramatic change at the end of sweep period is received, the LPD cannot recognize the sweep period of the different chirp-type interference. Furthermore, as a constant rate of frequency change model is used, a frequency tracking error may occur when the frequency change rate is not constant in the sweep period.

Second of all, an interference tracking algorithm is proposed that utilizes an adaptive hybrid EKF that is based on the Fourier series and also an order-reduction algorithm based on Powell's method to estimate the frequency of various chirp-type interferences. The proposed adaptive logic always guarantees the nonnegative aspect of the fading factor and reduces the measurement error effectively. In addition, the optimal order of the Fourier series for the signal type is selected by the proposed order-reduction algorithm. The revised frequency tracking algorithm which does not depend on estimating the sweep period is needed, to track the various chirp-type interferences. Simulation results show that, compared to conventional methods, the proposed algorithm does not have better tracking performance than PAKF with linear chirp-type interference, but it maintains tracking

performance regardless of the signal type. For chirp-type interference without dramatic changes and for nonlinear chirp-type interference, the proposed algorithm has better performance compared to that of AKF and PAKF due to the nonlinear filter state model designed using a Fourier series. The frequency estimation RMSE of the proposed algorithm is 0.0060, that of the AKF method is 0.0179, and that with the PKF is 0.0204 in the total cases of chirp-type interference.

In the last, with the interference tracking results, a mitigation method based on a notch filter is applied to eliminate the interference. The frequency tracking results are used to set the notch center frequency. By the notch filtering with infinite depth at the GPS signal frequency, the GPS information as well as the interference is removed. Thus, the adjust parameter of notch depth is added to the general notch filter. The mitigation performance is verified using a cross-ambiguity function to detect the presence of the GPS signal as the mitigated signal passes through the notch filter. According to simulation results, it is confirmed that the mitigation algorithm removes the interference components perfectly. Thus, the code phase and Doppler frequency of the GNSS satellite's one channel are obtained using the mitigated signal, and these results are identical to those of the original GPS signal.

The simulation results show that the proposed method can effectively detect GPS interference and mitigate its effect without GPS signal distortion. These proposed methods are expected to be useful for identifying jamming situations, and for selecting effective interference mitigation methods.

However, further works are needed for applying the proposed algorithm to a practical mitigation system. First of all, the process steps of the proposed algorithm should be reduced to decrease the computational time. One of the solution is using a Kalman notch filter which can simultaneously track and eliminate the interference frequency in the received signal. Secondly, stability of the Kalman notch filter should be analyzed in order to track the chirp-type interference, and a proper selection of initial parameters related to Kalman notch filter is important to consider the convergence rate of the filter. Lastly, the proposed algorithm would be extended to multi-target tracking algorithm for track the multiple chirp-type interference. The proposed algorithm in this dissertation can track and remove the single chirp-type interference in the received signal. However, in the real situation, there is a chance that various interference sources are in the received signal. Thus, the multi-state tracking filter is needed to track the various interference sources, and one of the filter is multi-target multi-Bernoulli filter.

Bibliography

[1] Balaei, A.T., Dempster, A.G (2009) A statistical inference technique for GPS interference detection. IEEE Trans. Aerosp. Electron. Syst. 45(4): 1499–1509. doi: 10.1109/TAES.2009.5310313

[2] Yang, J.H., Kang, C.H., Kim, S.Y., Park, C.G. (2012) Intentional GNSS interference detection and characterization algorithm using AGC and adaptive IIR notch filter. Int'l J. of Aeronautical & Space Sci. 13(4):491-498. doi: 10.5139/IJASS.2012.13.4.491

[3] Yang, J.H. (2013) GNSS Interference simulator design for RFI impact assessment and detection algorithm development. Master's Thesis, Seoul national University

[4] Chang, C.L., Juang, J.C. (2008) Effect of array configurations on the performance of GNSS interference suppression. International Journal of Control, Automation, and Systems 6(6):884-893

[5] Ward, P.W. (2008) Simple techniques for RFI situational awareness and characterization in GNSS receivers. Proc. ION NTM 2008, Institute of Navigation, 28-30 Jan. , San Diego, California, USA, pp. 154 – 163

[6] Betz, J.W. (2000) Effect of narrowband interference on GPS code tracking accuracy. Proc. ION NTM 2000, Institute of Navigation, 26-28 Jan. , Anaheim, California, USA, pp.16- 27

[7] Cho, N.I., Lee, S.U. (1993) On the adaptive lattice notch filter for the detection of sinusoids. IEEE Trans. Circuits Syst. 40(7): 405–416. doi: 10.1109/82.238368

[8] Choi, J.W., Cho, N.I. (2002) Suppression of narrow-band interference in DS-Spread spectrum systems using adaptive IIR Notch filter. Signal Process. 82(12): 2003–2013. doi: 10.1016/S0165-1684(02)00385-7

[9] Rusch, L.A., Poor, H.V. (1994) Narrowband interference suppression in CDMA spread spectrum communications. IEEE Trans. Commun. 42(234): 1969–1979. doi: 10.1109/TCOMM.1994.583411

[10] Borio, D., Camoriano, L., Presti, L.L. (2008) Two-pole and multi-pole notch filters: a computationally effective solution for GNSS interference detection and mitigation. IEEE Systems Journal 2(1): 38-47. doi:10.1109/JSYST.2007.914780

[11] Chien, Y.R., Huang, Y.C., Yang, D.N., Tsao, H.W. (2010) A novel continuous wave interference detectable adaptive notch filter for GPS receivers. GLOBECOM 2010, IEEE, 6-10 Dec. , Miami, FL, USA

[12] Capozza, P.T., Holland, B.J., Hopkinson, T.M., Landrau, R.L. (2000) A single-chip narrow-band frequency-domain excisor for a global positioning system (GPS) receiver. IEEE J. Solid-State Circuits 35(3): 401–411. doi: 10.1109/4.826823

[13] Thompson, R., Cetin, E., Dempster, A. (2011) Detection and jammer-to-noise ratio estimation of interferers using the automatic gain control. Proc. of IGNSS Symposium 2011, IGNSS, 15-17 Nov., Sydney, Australia.

[14] Borio, D.,O'driscoll, C., Fortuny, J. (2014) Fast and flexible tracking and mitigating a jamming signal with an adaptive notch filter, Inside GNSS, 9 (2)

[15] Kang, C. H., Kim, S. Y., Park, C. G. (2014) A GNSS interference identification and tracking based on adaptive fading Kalman filter. 19th *IFAC World Congress*, Aug. 24-29, Cape town, South Africa.

[16] Kaplan, E. D. (2006) Hegarty, Understanding GPS: principles and applications, Artech House, Norwood, MA.

[17] Pullen, S., . Gao, G., Tedeschi, C. and Warburton, J. (2012) The impact of uninformed RF interference on GBAS and potential mitigations. Proceedings of the 2012 ITM ION, Newport Beach, CA.

[18] Mitch, R. H., Dougherty, R. C., Psiaki, M. L., Powell, S. P., O'Hanlon, B. W., Bhatti, J. A., and Humphreys, T. E.(2011) Signal characteristics of civil GPS jammers, Proc. of the ION GNSS 2011, Sept. 2011, Portland, USA.

[19] Landry, R. J., and Renard, A. (1997) Analysis of potential interference sources and assessment of present solutions for GPS/GNSS receivers. 4th Saint-Petersburg on INS, 1-13.

[20] Trinkle, M., and Gray, D. (2001) GPS interference mitigation; overview and experimental results. In Proceedings of the 5th International Symposium on Satellite Navigation Technology & Applications

[21] Legrand, F., Macabiau, C., Issler, J. L., Lestarquit, L., and Mehlen, C. (2000) Improvement of pseudorange measurements accuracy by using fast adaptive bandwidth lock loops. ION GPS 2000, 13th International Technical Meeting of the Satellite Division of The Institute of Navigation.

[22] Przyjemski, J., Balboni, E., Dowdle, J., and Holsapple, B. (1993) GPS anti-jam enhancement techniques. In The 49th Annual Meeting on Future Global Navigation and Guidance, 41-50.

[23] Manz, A., Shallberg, K., and Shloss, P. (2000) Improving WAAS receiver radio frequency interference rejection. In Proceedings of the 13th International Technical Meeting of the Satellite Division of The Institute of Navigation (ION GPS 2000), 471-479.

[24] Parkinson, B. W. (1996) Progress in astronautics and aeronautics: global positioning system: Theory and Applications, American Institute of Aeronautics and Astronautics, Inc.

[25] Landry, R. (1999) New technique to improve GPS receiver performances by acquisition and tracking thresholds reduction. The 6th International Conference on Integrated Navigation Systems, St. Petersburg, Russia, 11-1.

[26] Regalia, P. A. (1995) Adaptive IIR filtering in signal processing and control. Marcel Dekker, New York

[27] Kang, C. H., Kim, S. Y., Park, C. G. (2014) A GNSS interference identification using an adaptive cascading IIR notch filter. GPS Solutions, 18(4), 605-613.

[28] Kang, C. H., Kim, S. Y., Park, C. G. (2015) Global navigation satellite system interference tracking and mitigation based on an adaptive fading Kalman filter. Radar, Sonar & Navigation, IET, 9(8), 1030-1039.

[29] Boashash, B. (2003) Time-freqeuncy analysis and processing, Elsevier.

[30] Sejdic, E., Stankovic, L., Dakovic, M., Jiang, J. (2008) Instantaneous frequency estimation using the S-transform, IEEE Signal Processing Letters, 15, 309-312

[31] Tsui, J. (2005) Fundamentals of global positioning system receivers. Wiley-Interscience, Hoboken.

[32] Saliu, S. (2000) Definition of instantaneous frequency on real signal, EUSIPCO, sept. 4-9, Tampere, Finland

[33] Xia, Q., Rao, M., Ying, Y., and Shen, X.(1994) Adaptive fading Kalman filter with an application, 30, (8), 1333-1338.

[34] Jwo, D. J., Weng, T. P.(2008) An adaptivee sensor fusion method with applications in integrated navigation, The Journal of Navigation, 61, 705-721

[35] Kim, K. H., Lee, J. G., Park, C. G.(2009) Adaptive two-stage extended Kalman filter for a fault-tolerant INS-GPS loosely coupled system, IEEE Trans. On Aerospace and Electronic Systems, 45, (1), 125-137

[36] Laguna, P., Thakor, N. V., Caminal, P., Jane, R., Yoon, H. R., Bayés de Luna, A., and Guindo, J. (1990) New algorithm for QT interval analysis in 24-hour Holter ECG: performance and applications, Medical and Biological Engineering and Computing, 28, (1), 67-73.

[37] Oikonomou, V. P., Tzallas, A. T., Fotiadis, D. I. (2007) A Kalman filter based methodology for EEG spike enhancement, Computer methods and programs in biomedicine, 85, (2), 101-108.

[38] Arnold, M., Milner, X. H. R., Witte, H., Bauer, R., and Braun, C. (1998) Adaptive AR modeling of nonstationary time series by means of Kalman filtering, IEEE Trans. On Biomedical Engineering, 45, (5), 553-562.

[39] Grenier, Y. (1983) Time-dependent ARMA modeling of nonstationary signals, IEE Trans. On ASSP, 31, (4), 899-911.

[40] Batistide, F., Akos, D., Macabiau, C., Roturier, B. (2003) Automatic gain control (AGC) as an interference assessment Tool. Proc. ION GNSS 2003, Institute of Navigation, 9 -11 Sep. Portland, OR, USA, 2042-2053

[41] Isoz, O., Akos, D., Lindgren, T. (2011) Assessment of GPS L1/Galileo E1 interference monitoring system for the airport environment. Proc. ION GNSS 2011, Institute of Navigation, 20-23 Sep., Portland, OR, USA, 1920-1930

[42] Toivonen, H. T., Hietarinta, L. (2015) Fourier state-space analysis of linear discrete-time periodic systems. Automatica, 53, 136-140.

[43] Mitch, R. H., Psiaki, M. L., Powell, S. P., O'Hanlon, B. W.. (2013) Signal acquisition and tracking of chirp-style GPS jammers. *Proceedings of the ION GNSS 2013*, Sep. 16-20, pp. 2893 - 2909, Nashville, TN

[44] Bitmead, R. R., Tsoi, A. C., Parker, P. J. (1986) A Kalman filtering approach to short-time Fourier analysis. *IEEE Transactions on Acoustics, Speech and Signal Processing*, 34 (6), 1493-1501.

[45] Simon, D. (2006) Optimal state estimation: Kalman, H infinity, and nonlinear approaches. John Wiley & Sons.

[46] Reif, K., Günther, S., Yaz, E., Unbehauen, R. (1999) Stochastic stability of the discrete-time extended Kalman filter. IEEE Transactions on Automatic Control, 44(4), 714-728.

[47] Agniel, R. G., Jury, E. I. (1971) Almost sure boundedness of randomly sampled systems. SIAM Journal on Control, 9(3), 372-384.

[48] Anderson, B. D. O., Moore, J. B. (1981) Detectability and stabilizability of time-varying discrete-time linear systems. SIAM Journal on Control and Optimization, 19(1), 20-32.

[49] Goodwin, G. C., Sin, K. S. (1984) Adaptive filtering prediction and control. Englewood Clifs: Prentice Ha 11.

[50] Morozan, T. (1968) Stability of stochastic discrete systems. Journal of Mathematical Analysis and Applications, 23(1), 1-9.

[51] Tarn, T. J., Rasis, Y. (1976) Observers for nonlinear stochastic systems. Automatic Control, IEEE Transactions on, 21(4), 441-448.

[52] Johnson, M. L., Correia, J. J., Yphantis, D. A., HalvorSON, H. R. (1981) Analysis of data from the analytical ultracentrifuge by nonlinear least-squares techniques. Biophysical Journal, 36(3), 575.

[53] Fitzgibbon, A., Pilu, M., Fisher, R. B. (1999) Direct least square fitting of ellipses. Pattern Analysis and Machine Intelligence, IEEE Transactions on, 21(5), 476-480.

[54] Jiade, T. (2008) Nonlinear curve fitting based on MATLAB. Comput. Modern, 154(6), 15-19.

[55] Suh, Y. S. (2010) Orientation estimation using a quaternion-based indirect Kalman filter with adaptive estimation of external acceleration. *IEEE Transactions on Instrumentation and Measurement*, vol. 59, no.12, pp. 3296-3305.

[56] Porikli, F., Tuzel, O., Meer, P. (2006) Covariance tracking using model update based on lie algebra. In Computer Vision and Pattern Recognition, 2006 IEEE Computer Society Conference on (Vol. 1, pp. 728-735). IEEE.

[57] Hide, C., Moore, T., Smith, M. (2003) Adaptive Kalman filtering for low-cost INS/GPS. The Journal of Navigation, 56(01), 143-152.

[58] Sabatini, A. M. (2006) Quaternion-based extended Kalman filter for determining orientation by inertial and magnetic sensing. Biomedical Engineering, IEEE Transactions on, 53(7), 1346-1356.

[59] Jetto, L., Longhi, S., Venturini, G. (1999) Development and experimental validation of an adaptive extended Kalman filter for the localization of mobile robots. Robotics and Automation, IEEE Transactions on, 15(2), 219-229.

[60] Mohamed, A. H., Schwarz, K. P. (1999) Adaptive Kalman filtering for INS/GPS. Journal of geodesy, 73(4), 193-203.

[61] Li, W., Sun, S., Jia, Y., Du, J. (2016) Robust unscented Kalman filter with adaptation of process and measurement noise covariances. Digital Signal Processing, 48, 93-103.

[62] Golub, G. H., Reinsch, C. (1970) Singular value decomposition and least squares solutions. *Numerische mathematik*, 14(5), 403-420.

[63] Cao, L., Schwartz, H. M. (2004) Analysis of the Kalman filter based estimation algorithm: an orthogonal decomposition approach. Automatica, 40(1), 5-19.

[64] Yu, M. J. (2012) INS/GPS integration system using adaptive filter for estimating measurement noise variance. IEEE Transactions on Aerospace and Electronic Systems, 48(2), 1786-1792.

[65] Nelder, J. A., Mead, R. (1965) A simplex method for function minimization. The computer journal, 7(4), 308-313.

[66] Maes, F., Vandermeulen, D., Suetens, P. (1999) Comparative evaluation of multiresolution optimization strategies for multimodality image registration by maximization of mutual information. Medical image analysis, 3(4), 373-386.

[67] Arouxét, M., Echebest, N., Pilotta, E. A. (2011) Active-set strategy in Powell's method for optimization without derivatives. Computational & Applied Mathematics, 30(1), 171-196.

[68] Li, C. J., LILAI, Y., Chbat, N. W. (1995) Powell's method applied to learning neural control of three unknown dynamic systems. Optimal control applications & methods, 16(4), 251-262.

[69] Asaadi, J. (1973) A computational comparison of some non-linear programs. Mathematical Programming, 4(1), 144-154.

[70] Fletcher, R. (2013) Practical methods of optimization. John Wiley & Sons.

[71] Brent, R. P. (2013) Algorithms for minimization without derivatives. Courier Corporation.

[72] Powell, M. J. D. (1982) Nonlinear optimization 1981. In NATO Conference Series. Series II: Systems Science, Proceedings of the NATO Advanced Research Institute, held at Cambridge (UK), July, 1981, London: Academic Press, 1982, edited by Powell, MJD (Vol. 1).

[73] Vanderplaats, G. N. (1984) Numerical optimization techniques for engineering design: with applications. New York: McGraw-Hill.

[74] Venkataraman, P. (2009) Applied optimization with MATLAB programming. John Wiley & Sons.

[75] Luo, M., Xie, G., Akos, D., Pullen, S., Enge, P. (2003) Radio frequency interference validation testing for LAAS using the Stanford Integrity Monitor Testbed. In Proceedings of the Institute of Navigation National Technical Meeting, Anaheim, CA.

[76] Brown, A., Atterberg, S., Gerein, N. (2000) Detection and location of GPS interference sources using digital receiver electronics. In Proceedings of ION Annual Meeting. San Diego, CA

[77] Brown, A., Reynolds, D., Roberts, D., Serie, S. (1999) Jammer and interference location system design and initial test results. In Proceedings of the ION GPS, Nashville, TN.

[78] Ward, P. W. (2001) Simple techniques for RFI situational awareness and characterization in GNSS receivers. In Proceedings of the 2008 National Technical Meeting of The Institute of Navigation, San Diego, CA

[79] Ndili, A., Enge, P. (1998). GPS receiver autonomous interference detection. In Position Location and Navigation Symposium, IEEE, Palm Springs, CA

[80] Yun, Y., Kee, C., Rife, J., Luo, M., Pullen, S., Enge, P. (2006) Detecting RFI through integrity monitoring at a DGPS reference station. Journal of Navigation, 59(03), 403-422.

[81] Balaei, A. T., Dempster, A. G., and Barnes, J. (2006) A novel approach in detection and characterization of CW interference of GPS signal using receiver estimation of C/No. PLANS, San Diego, CA.

[82] Marti, L. M. (2004) Global positioning system interference and satellite anomalous event monitor. Doctor of Philosophy Thesis, College of Engineering and Technology of Ohio University

[83] Kang, C. H., Kim, S. Y., Yang, J. H., Park, C. G.(2012) Detection and characterization algorithm of swept continuous wave interference for safe GBAS operation, Proc. of the ION GNSS 2012, Nashville, USA, Sept., 3465-3470

[84] Rusch, L. A., Poor, H. V.(1994) Narrowband interference suppression in CDMA spread spectrum communications', IEEE Trans. On Commun., 42, pp. 1969-1979

[85] Mitra, S. K., Kuo, Y. (2006) Digital signal processing: a computer-based approach. New York: McGraw-Hill.

[86] Sameni, R. (2012) A linear kalman notch filter for power-line interference cancellation. In Artificial Intelligence and Signal Processing (AISP), 2012 16th CSI International Symposium on. IEEE. Shiraz

[87] Borre, K., Akos, D. M., Bertelsen, N., Rinder, P., and Jensen, S. H. (2007) A software-defined GPS and Galileo receiver: a single-frequency approach. Springer Science & Business Media.

[88] Grewal, M. S., Andrews, A. P., and Filtering, A. K. (2001) Theory and practice using Matlab. Wieley-Interscience, Canada.

국문초록

위성항법신호는 지상에서 수신할 때 신호의 세기가 약해서 수신된 위성항법신호보다 상대적으로 신호세기가 큰 전파신호에 의해서 쉽게 전파교란 효과를 받을 수 있다. 2011 년 서해안 지역에서 전파교란 신호가 발생하여 이동통신사 및 항공사 등에서 위성항법신호를 사용하는 장비가 제대로 작동되지 않아서 심각한 문제를 야기하였는데, 전파교란에 쓰인 신호 형태가 단일 주파수 형태와 전파간섭 신호의 중심주파수가 이동 (sweeping) 하는 형태였음을 확인하였다. 이러한 위협에 대비하기 위해서 국내외 많은 연구팀들이 연구 중에 있으며, 기존의 연구들이 단일 주파수 형태의 전파간섭 신호 검출에 초점이 맞춰졌다면 최근에는 위의 사례와 같이 신호의 중심주파수가 이동하는 형태의 신호에 대해서 전파간섭 영향을 평가하고 분석하는데 주력하고 있다. 특히 미국 코넬대 연구팀에서 발표한 논문에서 휴대용 전파간섭 신호 생성기 (portable jammer) 대부분이 중심주파수가 이동하는 형태의 신호 파형을 가지는 것을 확인하였고, 이를 chirp 형태의 전파간섭 신호로 분류하고 있다. 기존의 노치필터 (notch filter) 기반의 전파간섭 신호 검출 기법으로는 중심주파수가 변화하는 신호를 정확하게 검출 및 추적 할 수 없으며, 효율적으로 이러한 전파간섭 신호에 대응을 할 수 없다.

따라서 본 논문에서는 위성항법시스템에 영향을 주는 전파간섭 신호 중 chirp 형태의 전파간섭 신호를 검출하고 추적하는 시간-주파수 영역 기법 두 가지를 제안하였다. 제안한 기법은 선형 chirp 신호에 대응할 수 있는 것과 비선형 chirp 신호에 대응할 수 있는 것으로 분류할 수 있고, 먼저

선형 chirp 신호에 대응하기 위해서 chirp 신호의 주기를 추정하는 알고리즘과 추정된 주기마다 필터 상태변수를 초기화하는 알고리즘을 구현하여 주파수 추적 성능을 향상시켰다. Chirp 신호의 주기를 추정하기 위해서 저역통과 미분기 (low pass differentiator)와 패턴인식 알고리즘을 사용하였다. 비선형 chirp 신호 주파수 추적을 위해서 퓨리에 급수 (Fourier series) 로 측정 주파수를 모델링 하였고 추적성능 향상을 위해서 오차 공분산을 재추정하는 알고리즘을 추가하였다.

위의 주파수 추적 결과를 이용하여 본 논문에서는 chirp 신호를 수신신호에서 제거하는 노치 필터 기반의 알고리즘을 구현하였으며 위성항법신호 왜곡을 최소화하기 위해서 노치 깊이를 조절하는 알고리즘을 추가하였다. 다양한 시뮬레이션을 통해 세가지 chirp 형태의 전파간섭 신호를 추적하는 것을 확인하였고 추적한 전파간섭 신호를 수신신호에서 제거 후에 위성항법신호가 제대로 수신되는 것을 확인하였다.

주요어: GPS 전파간섭 신호 추적 및 완화기법, 적응칼만필터, 적응노치필터, 퓨리에 급수

이 름: 강 창 호

학 번: 2009-23059